MASSACHUSETTS INSTITUTE OF TECHNOLOGY
LINCOLN LABORATORY

THE COBEL MODEL AS PART OF A TERMINAL-AREA CEILING & VISIBILITY (C&V) NOWCAST SYSTEM: A PROGRESS REPORT

R. TARDIF
M. BEAUCHEMIN
P. ZWACK
Agent de recherche & planification
Groupe de Sciences de l'Atmosphere
Departement des Sciences de la Terre
Universite du Quebec a Montreal
J.L. KELLER
Group 43

PROJECT REPORT ATC-241

18 JULY 1996

LEXINGTON MASSACHUSETTS

TECHNICAL REPORT STANDARD TITLE PAGE

1. Report No.	2. Government Accession No.	3. Recipient's Catalog No.
ATC-241		

4. Title and Subtitle	5. Report Date
The COBEL Model as Part of a Terminal-Area Ceiling & Visibility (C&V) Nowcast System: A Progress Report	18 July 1996
	6. Performing Organization Code
7. Author(s)	8. Performing Organization Report No.
Robert Tardif, Maryse Beauchemin, Peter Zwack, and John L. Keller	ATC-241
9. Performing Organization Name and Address	10. Work Unit No. (TRAIS)
Lincoln Laboratory, MIT 244 Wood Street Lexington, MA 02173-9185	11. Contract or Grant No. DTFA01-91-Z-02036
12. Sponsoring Agency Name and Address	13. Type of Report and Period Covered
Department of Transportation Federal Aviation Administration Washington, DC 20591	Project Report
	14. Sponsoring Agency Code

15. Supplementary Notes

This report is based on studies performed at Lincoln Laboratory, a center for research operated by Massachusetts Institute of Technology under Air Force Contract F19628-95-C-0002. The studies by Tardif, Beauchemin, and Zwack were performed under Lincoln Laboratory Contract No. BX-5187.

16. Abstract

The Federal Aviation Administration (FAA) Integrated Terminal Weather System (ITWS) is supporting the development of products aimed at providing automated guidance to the air traffic managers for the anticipation of changes in ceiling and visibility (C&V) conditions and wake vortex behavior in the terminal area. Fine resolution, one-dimensional (column) numerical models are being considered to provide information on the evolution of the local fine-scale structure of the lower atmosphere over the terminal area. The COde Brouillard Eau Liquide (COBEL) column model is being investigated for potential use within the ITWS. This one-dimensional numerical model has been developed for the short-term prediction of fog events in the north of France.

This report describes initial progress in adapting the COBEL model to a wider range of meteorological conditions. A parameterization of surface frost deposition was implemented and a slight error in the computation of stability in a saturated atmosphere was corrected. Tests suggest that these modifications represent important features of the newest version of the COBEL model. Other significant modifications to the COBEL model were performed. Pressure tendencies and vertical motion (vertical advection) were implemented as additional external forcings to the column model. Sensitivity tests show that these forcings play important roles in determining the onset, evolution, and dissipation of low stratiform clouds. Some further applications of the model are briefly discussed and future developments are suggested.

17. Key Words			18. Distribution Statement
fog	stratus	column model	This document is available to the public through the National Technical Information Service, Springfield, VA 22161.
radiation	fluxes	aviation weather	
ceiling	visibility	ITWS	
vertical structure			

19. Security Classif. (of this report)	20. Security Classif. (of this page)	21. No. of Pages	22. Price
Unclassified	Unclassified	58	

FORM DOT F 1700.7 (8-72) Reproduction of completed page authorized

ABSTRACT

The Federal Aviation Administration (FAA) Integrated Terminal Weather System (ITWS) is supporting the development of products aimed at providing automated guidance to the air traffic managers for the anticipation of changes in ceiling and visibility (C&V) conditions and wake vortex behavior in the terminal area. Fine-resolution, one-dimensional (column) numerical models are being considered to provide information on the evolution of the local fine-scale structure of the lower atmosphere over the terminal area. The COde Brouillard Eau Liquide (COBEL) column model is being investigated for potential use within the ITWS. This one-dimensional numerical model has been developed for the short-term prediction of fog events in the north of France.

This report describes initial progress in adapting the COBEL model to a wider range of meteorological conditions. A parameterization of surface frost deposition was implemented and a slight error in the computation of stability in a saturated atmosphere was corrected. Tests suggest that these modifications represent important features of the newest version of the COBEL model. Other significant modifications to the COBEL model were performed. Pressure tendencies and vertical motion (vertical advection) were implemented as additional external forcings to the column model. Sensitivity tests show that these forcings play important roles in determining the onset, evolution and dissipation of low stratiform clouds. Some further applications of the model are briefly discussed and future development efforts are suggested.

EXECUTIVE SUMMARY

The Federal Aviation Administration (FAA) Integrated Terminal Weather System (ITWS) is supporting the development of products aimed at providing automated guidance to the air traffic managers for the anticipation of changes in ceiling and visibility (C&V) conditions and wake vortex behavior in the terminal area. A Dynamic Atmospheric Vertical Structure Nowcast System is being developed to provide current and very short-term predictions of the vertical structure of the lower atmosphere at strategic sites in the terminal area. The core of this system would be a high-resolution one-dimensional (1D) boundary layer model. Efforts described and discussed in this document represent important groundwork concerning future development efforts, such as adapting the ***CO***de ***B***rouillard ***E***au ***L***iquide (COBEL) technology toward an improvement of its versatility, and thus to its possible use within the ITWS.

The Massachusetts Institute of Technology Lincoln Laboratory (MIT/LL) has been collaborating with members of the Atmospheric Sciences group at the Université du Québec à Montréal (UQAM) for the evaluation of the COBEL column model. This one-dimensional numerical model has been developed at the Laboratoire d'Aérologie, Université Paul Sabatier in Toulouse France for the short-term prediction of fog events in the north of France. Its potential use within the FAA Integrated Terminal Weather System is being investigated. The COBEL model has originally been designed to represent the local fine-scale structure of the lower atmosphere. The main characteristics of this model are : (i) a turbulent mixing parameterization based on turbulent kinetic energy and adaptation to the nocturnal lower atmosphere; (ii) a high spectral resolution longwave radiation scheme; (iii) a simple parameterization for microphysics; and (iv) a representation of soil-atmosphere exchange for heat and moisture [1]. COBEL's high-resolution, long-wave radiation model permits an accurate depiction of thermal radiation, while its sophisticated turbulence parameterization is needed in order to realistically represent turbulent exchanges in the stable nocturnal atmospheric boundary layer. A great number of published studies suggest that the accurate representation of these two factors (radiation and turbulence) is crucial to a successful simulation of changes in ceiling and visibility conditions. Also, the close relationship between turbulence intensity and wake vortex behavior suggests that COBEL predictions of turbulent kinetic energy represent a desirable capability for a wake vortex advisory system.

Météo-France is developing a system using the COBEL model, driven by pressure forces and horizontal advections, to predict the formation of dense radiation fog. An experimental version of the model, driven by *observed* horizontal advections and high cloud cover, has been successfully tested on several observed fog cases in France's Nord-Pas de Calais region [2]. A pre-operational version of COBEL, driven by horizontal advections and cloud cover taken from an operational limited area mesoscale model, has also been successfully tested at Météo-France over a greater number of fog cases [3].

Efforts in adapting the COBEL model to a wider range of meteorological conditions has recently been undertaken by UQAM-MIT/LL. First, the implementation of a solar radiation parameterization scheme has allowed the simulation of the daytime boundary layer evolution. Preliminary tests showed that COBEL performed realistically when applied to the solar energy induced dissipation of a fog layer [4]. Subsequent modifications were introduced in the model after a review of the computer code in which some features were found to be missing or seemed

to be inconsistent with the ongoing or future development plans. The computation of soil-atmosphere exchanges of water vapor was slightly modified to add the capability of representing the *frost* deposition process. In the original version, only the effects of *dew* deposition were taken into account. It is shown that this addition plays an important role in the prediction of visibility near the ground. Also, some errors in the computation of stability in a saturated atmosphere within COBEL were rectified. Since errors induced are small near the surface but become larger with height, the impact on fog prediction is negligible. Tests suggest that previous estimates of stability may not have been realistic in other scenarios, such as stratus or stratocumulus prediction.

ACKNOWLEDGMENTS

We wish to acknowledge the cooperation of Professor Daniel Guedalia of Paul Sabatier University for providing the original source code to UQAM and for his personal consultations in helping us to understand its complex algorithms. In addition, we thank Meteo France for hosting Robert Tardif during his visit to Lille, France to assimilate the COBEL software for its subsequent evaluation. Others also played a role in the evaluation of the COBEL, especially Chris Smith of MIT Lincoln Laboratory for help in hosting the COBEL source code on our Laboratory's computers.

TABLE OF CONTENTS

LIST OF ILLUSTRATIONS

Preceding Page Blank

LIST OF ILLUSTRATIONS (CONTINUED)

LIST OF TABLES

1. INTRODUCTION

This document is set in the context of the Massachusetts Institute of Technology Lincoln Laboratory ongoing collaboration with the Université du Québec à Montréal for the adaptation of the COBEL (***CO***de ***B***rouillard ***E***au ***L***iquide) column model as a potential tool within the Federal Aviation Administration (FAA) Integrated Terminal Weather System (ITWS). It is now recognized that the nesting within a three-dimensional mesoscale model of a one-dimensional (1D) high vertical resolution boundary layer (BL) model is a viable alternative to the current problem of BL cloud forecasting [5] and thus to the production of enhanced ceiling and visibility (C&V) forecasts. This alternative has been chosen and exploited by Météo-France in collaboration with the Laboratoire d'Aérologie, Université Paul Sabatier in Toulouse France for the short-term prediction of fog events in the north of France. The central feature of Météo-France's system is the COBEL model, a high-resolution 1D nocturnal BL model developed at the Laboratoire d'Aérologie (Bergot and Guédalia, 1994). The main characteristics of this model are: (i) a turbulent mixing parameterization adapted to strong stable stratification (e.g., nighttime); (ii) a high-spectral-resolution longwave radiation scheme; (iii) a simple parameterization for microphysics; and (iv) a representation of soil-atmosphere exchange for heat and moisture.

The main underlying hypothesis for the work presented here is that enhanced C&V nowcasts can be produced using a high-resolution 1D model driven with detailed observations provided by ITWS' various sensors, and that very short term outlooks can also be provided to the aviation community by using a mesoscale model to drive the same 1D model. COBEL is an attractive alternative as the 1D numerical prediction component of this system mainly because of its 1.5 order turbulence closure scheme and its sophisticated radiation schemes. Also, the low computer cost associated to its use makes it a viable engine for the production of frequently updated forecasts.

An experimental version of COBEL, forced by *observed* horizontal advections and high cloud cover, has been successfully tested on several observed fog cases in France's Nord-Pas de Calais region [2]. A pre-operational version of the model, forced by horizontal advections and cloud cover taken from an operational mesoscale model, has also been successfully tested over a greater number of fog cases collected during three consecutive winters [3]. An overall 90 percent success rate has been obtained on all no-fog and fog cases during these three winters. Eighty-five percent of observed fog cases have been correctly predicted, with a false-alarm rate of 25 percent. These results show a dramatic improvement compared to fog forecasts performed by Météo-France's forecasters on the same cases (e.g., 67 percent detection rate and 57-percent false-alarm rate). Also, it was determined that the majority of COBEL's missed cases were related to errors in the mid- and high-level cloud cover forecasts produced with the mesoscale model used to drive the column model. With these good preliminary results, plans are under way to implement COBEL in an operational environment at Météo-France's Direction Interrégional Nord. A second operational application is under way at the Institut Royal Météorologique de Belgique, where the coupling of COBEL with an expert system is being considered for the forecasting of dense fog events at the Brussels airport. A detailed description of the initial formulation of the model can be found in [6].

Here, a discussion is presented on the latest modifications implemented in the model. Some changes were made after a review of the COBEL computer code in which some features were found to be missing or seemed to be inconsistent with the ongoing or future development plans. It was decided to implement and test corrections to these problems and to study their impact on the performance of the model. To continue the work of adapting the COBEL model to a wider range of meteorological scenarios, started by [4] with the implementation of the [7] solar radiation scheme, work on the implementation of a more complete set of dynamical external forcings has been undertaken. The effects of local pressure tendencies and vertical motion (w=dz/dt) are now included in COBEL's one-dimensional simulation. Details concerning this implementation and some results from sensitivity studies are presented in this document. These results suggest that, with the new implemented features, the COBEL model becomes an attractive tool for predicting transitions of stable-neutral-stable stratification during instrument flight rules (IFR) conditions at Dallas/Fort Worth International Airport (DFW).

2. DESCRIPTION OF MINOR MODIFICATIONS

While studying the code and comparing it with the available documentation, some discrepancies were found. It was discovered that the COBEL version used at UQAM did not incorporate the parameterization of surface *frost* deposition, as documented in [8]. Also, it was discovered that some aspects of the computation of stability in a saturated atmosphere might lead to erroneous estimates of stability in simulated fog layers. These aspects are discussed more fully in Section 2.2. Furthermore, it was discovered that parameters needed for the computation of stability, which is itself needed in the integration of the turbulent kinetic energy budget equation process, were used in a somewhat inconsistent manner.

2.1 Frost Deposition

Following the discovery that the frost deposition parameterization documented in [8] was not part of the version used at UQAM, it was decided that in order to have a version of the model that is as complete as possible, a suitable parameterization, based on the information found in [8], should be implemented.

Bergot [8] points out that when the surface temperature becomes lower than the freezing point, frost deposition occurs instead of dew deposition. Also, he indicates that *the rate at which frost deposition occurs is faster than the one associated with dew deposition.* Thus, to represent this effect, the saturation mixing ratio with respect to liquid water ($q_{sat}(T_{so})$) considered within the surface latent heat flux parameterization (see [8] and [6]) is changed to:

$$q_{sat_{frost}}(T_{so}) = q_{sat}(T_{so}) \frac{e_{is}(T_{so})}{e_{ws}(T_{so})} \tag{1}$$

where $e_{is}(T_{so})$ is the saturation vapor pressure over ice and $e_{ws}(T_{so})$ is the saturation vapor pressure over water at surface temperature T_{so}. Thus, a simple correction, represented by the ratio of e_{is} and e_{ws}, is applied to the computed saturation water vapor mixing ratio (q_{sat}) to represent the difference between the saturation state with respect to ice as compared to the one with respect to liquid water.

Within COBEL, to ensure the numerical stability of the scheme, the parameterized surface water vapor flux is linearized following [9]:

$$E = \rho C_h \left[q_{z1}^t - Hu \left(q_{sat}\left(T_{so}^t\right) + \frac{\partial q_{sat}}{\partial T}\left(T_{so}^{t+1} - T_{so}^t\right) \right) \right] \tag{2}$$

where superscripts indicate at which time step the surface temperature is considered (t = current time step, t+1 = next time step). q_{z1}, ρ and T represent the atmospheric water vapor mixing ratio at the lowest model level (0.5 m), air density and temperature, respectively. C_h is an exchange coefficient deduced from the Monin-Obukhov similarity theory [6] and Hu is the surface relative humidity. The applied correction to q_{sat} (eq. (1)) is used in this linearization procedure by

substituting eq. (1) in eq. (2), thus obtaining the expression of the water vapor flux resulting in surface frost deposition:

$$E_{frost} = \rho C_h \left[q_{z1}^t - Hu \left(q_{sat}\left(T_{so}^t\right) \frac{e_{is}\left(T_{so}^t\right)}{e_{ws}\left(T_{so}^t\right)} + \left(\frac{\partial q_{satfrost}}{\partial T} \right) \left(T_{so}^{t+1} - T_{so}^t \right) \right) \right] \quad (3)$$

where

$$\frac{\partial q_{satfrost}}{\partial T} = \frac{e_{is}\left(T_{so}^t\right)}{e_{ws}\left(T_{so}^t\right)} \frac{\partial q_{sat}}{\partial T} + q_{sat}\left(T_{so}^t\right) \left[\frac{e_{ws}\left(T_{so}^t\right) \frac{\partial e_{wi}}{\partial T} - e_{wi}\left(T_{so}^t\right) \frac{\partial e_{ws}}{\partial T}}{\left(e_{ws}\left(T_{so}^t\right)\right)^2} - \right] \quad (4)$$

is obtained by differentiating eq. (1) with respect to temperature (T).

Furthermore, the latent heat of vaporization is replaced by the latent heat of sublimation when frost deposition occurs. Since *the latent heat of vaporization (L_v) is already computed as a function of temperature within COBEL* [10], the latent heat of sublimation (L_s) is computed as a function of L_v using the following relation:

$$L_s = F_c L_v \quad (5)$$

where F_c is a temperature dependent factor. The dependency of F_c with temperature was deduced using values of L_s and L_v presented in Table 2.1 of [10]. This table is partially reproduced below (Table 1). A linear regression between F_c and temperature T results in the following relationship:

$$F_c = 0.001 \cdot T + 1.13 \quad (6)$$

Thus, the latent heat of sublimation (L_s) can be easily obtained by substituting eq. (6) into eq.(5). The *surface* temperature taken within COBEL is used to compute L_v, as well as F_c and thus L_s.

These expressions ((3), (4) and (5)) are used only when conditions favorable to *frost* deposition (downward flux) are diagnosed in the course of a simulation. For an upward water vapor flux, when the surface temperature is below 0°C, expressions (3) to (6) are also used. The only differences are the use of a different exchange coefficient C_h in (3) and a different surface relative humidity parameter (Hu). In the case of an upward flux, C_h is formulated using "K-theory" [4] instead of Monin-Obukhov similarity relationships which are used for the computation of the downward flux [6]. As far as the relative humidity parameter (Hu) is concerned, different values are used whether a downward ($Hu_{depo.}$) or an upward ($Hu_{evap.}$) flux is occurring.

Table 1
Latent Heats of Vaporization (L_V) and Sublimation (L_S), and Their Ratios (F_C) [10]

T (°C)	L_V (J/g)	L_S (J/g)	F_C (=L_S/L_V)
-40	2603	2839	1.09
-30	2575	2839	1.10
-20	2549	2838	1.11
-10	2525	2837	1.12
0	2501	2834	1.13

When a downward water vapor flux occurs, $Hu_{depo.}$ is set to 1 (independent of the surface humidity) since it is assumed that the flux is controlled by the atmosphere. When an upward flux occurs, it is mainly controlled by the hydrological state of the soil surface. Thus, the surface relative humidity parameter ($Hu_{evap.}$) must be dependent on the saturation state of the soil surface, with $0 \leq Hu_{evap.} \leq 1$ [4]. Within COBEL, the same value of $Hu_{evap.}$ (or $Hu_{depo.}$) is used regardless of the fact that the surface temperature is below or above the freezing point.

To illustrate these considerations, the modified general algorithm for the surface water vapor flux is presented in Figure 1. To summarize, first a test is performed to see if the surface temperature (T_{so}) is below 0° C. If it is, then the e_{is}/e_{ws} correction to q_{sat} is used along with the water vapor mixing ratio at the lowest model level (q(1)) in order to diagnose whether conditions are favorable to a downward or an upward water vapor flux. Then, relevant relations are used to compute the surface water vapor flux. If the surface temperature is above the freezing point, similar steps and computations are performed, but without using the e_{is}/e_{ws} correction to q_{sat}. If conditions for an upward or a downward water vapor flux are not met, the flux is simply set to zero.

2.2 Stability in a Saturated Atmosphere

In the presence of liquid water, the stability criteria considered within COBEL is derived from the formulation of the Brünt-Vaïsälä frequency of [11], where the vertical temperature gradient is now expressed with the use of potential temperature (equation (24) of [6]:

$$\left[\frac{T}{\theta}\frac{d\theta}{dz}+\Gamma_m-\frac{g}{c_p}\right]\left[1+\frac{Lq_{sat}(T)}{RT}\right]-\frac{T}{1+q_w}\frac{dq_w}{dz}\begin{cases}<0 \text{ unstable}\\ =0 \text{ neutral}\\ >0 \text{ stable}\end{cases} \quad (7)$$

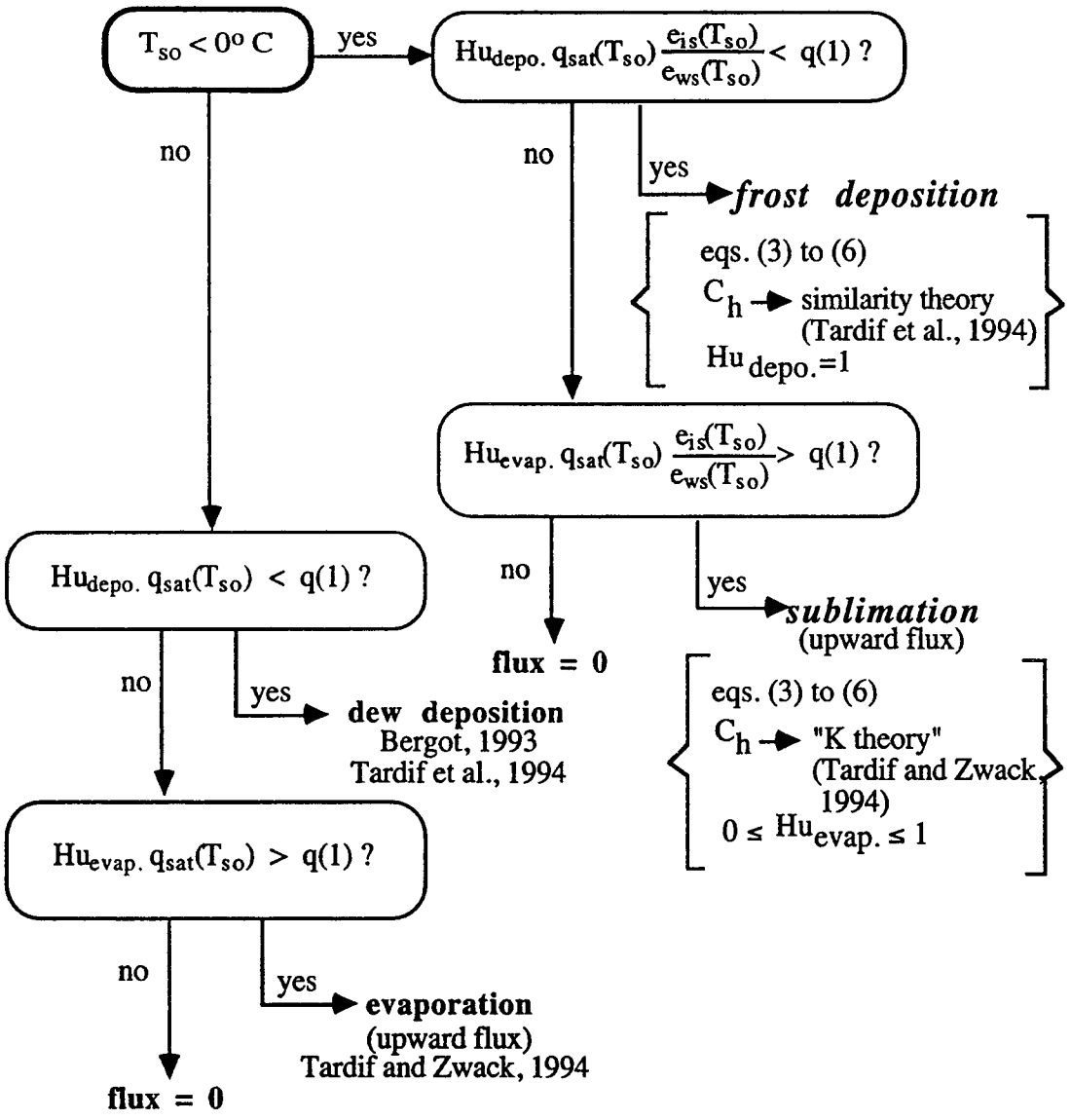

Figure 1. Schematic representation of the surface water vapor flux algorithm.

In (7), q_w is the total water mixing ratio and Γ_m is the pseudo-adiabatic lapse rate [12]:

$$\Gamma_m = \Gamma_d \left[(1+q_{sat}) \frac{1+\frac{L\, q_{sat}}{R_d T}}{1+\frac{q_{sat}}{C_{pa}} \left(C_{pv} + \frac{L^2}{R_v T^2} \left(1+q_{sat} \frac{R_v}{R_d} \right) \right)} \right] \qquad \textbf{(8)}$$

where q_{sat} is computed with:

$$q_{sat} = 0.622 \frac{e_{ws}(T)}{p - e_{ws}(T)} \tag{9}$$

While studying the model code it became apparent that some aspects of the computation of eq. (7) were implicitly related to radiation fog forecasting and that they might not be realistic in other scenarios, such as stratus or stratocumulus forecasting. For example, the value of temperature T used to compute $e_{ws}(T)$, itself used to compute Γ_m (eq. (8)) and q_{sat} (eq. (9)), *was not explicitly computed in the computer program.* Tests on the computer used at UQAM showed that this resulted in the use of a constant value of 0 °C. Also, the pressure p used in the computation of q_{sat} (eq. (9)) *was set constant at 1000 hPa.* In the context in which the model has been used so far, these values can be considered valid or realistic, since stability in the presence of liquid water was computed only near the surface (fog -> near surface processes). It was believed that with these parameters, the computation of stability in the presence of liquid water for layers located higher up in the model domain could be somewhat deficient. So, in order to have as universal a model code as possible, it was decided to implement some modifications. Now, *explicitly computed mean layer temperature values and hydrostatic pressure values are used to compute q_{sat} and Γ_m throughout the model domain.*

Another important item, the *T/θ term within the first term on the left-hand side of (7) was missing*. Since the surface pressure was set at 1000 hPa in the model, this term is close to 1 in the first few tens of meters of the atmosphere. Consequently, it is believed that this term does not play an important role in the diagnosis of stability during the formation stage of a fog layer. But, as the fog layer grows in height and eventually becomes a stratus layer during the burn-off process, the introduction of the T/θ term might prove to be important. With pressure held constant in time, the magnitude of T/θ stays close to 1 in the lowest few meters of the atmosphere, but slowly decreases with height as shown in Figure 2. As a result, the relative importance of terms included in eq. (7) will be slightly different, thus possibly affecting the computation of stability near fog/stratus top as the cloud rises. Consequently, the complete expression of stability in a saturated atmosphere (eq. (7)) was implemented within the model. A validation of this modification is presented in Section 3.2.

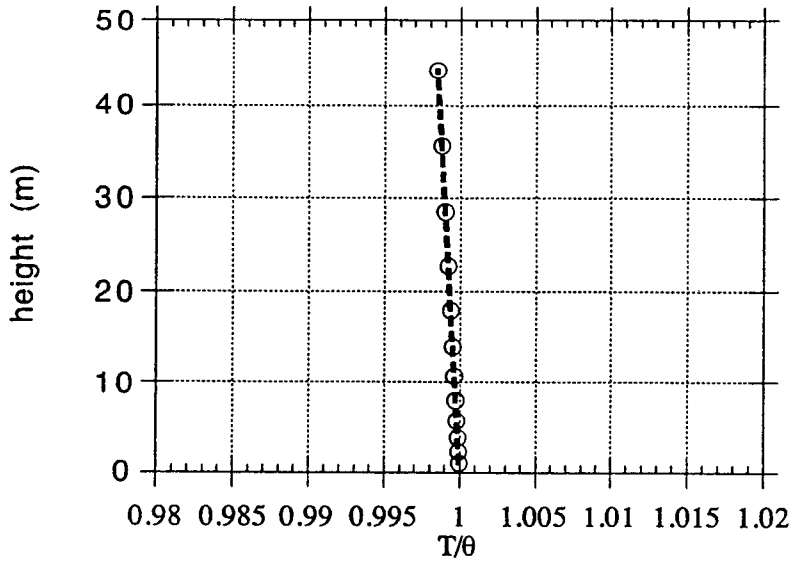

Figure 2. Mean magnitude of T/θ as a function of altitude within the fog layer, diagnosed at 0600 UTC November 16th (simulation of the November 15th-16th "Lille 88" case).

2.3 Turbulent Kinetic Energy Integration

Again while studying the model code, a time inconsistency was discovered in parameters involved in the computation of stability in a saturated atmosphere, used when solving the Turbulent Kinetic Energy (TKE) budget equation. In the COBEL model, each prognostic variable is solved one at a time (a form of process splitting), starting with potential temperature (θ), water vapor mixing ratio (q), wind components (u,v), liquid water (q_l) and then TKE. After each equation is solved, the variable contains the corresponding *updated* value (value at time "t+Δt"). In the model code, to solve the TKE budget equation, equation (7) is evaluated after updated values of θ, q, u,v, and q_l have been computed. But, values *valid at time "t"* of θ and thus of T were used, while *updated* values of q and q_l (q_w=q+q_l) (valid at time "t+Δt") were considered. In the context of COBEL stability is considered as a diagnostic parameter (valid at time "t"), thus that procedure seemed inconsistent. With COBEL's small time steps (30 sec. when liquid water has appeared), it is believed that this situation is not critical. Nevertheless, the code has been modified so that all parameters involved in the computation of equation (7) are taken at time "t".

3. TESTS AND VALIDATION OF MINOR MODIFICATIONS

3.1 Frost Deposition

The modified algorithm for surface exchanges of water vapor described in Section 2.1 is tested using simulations of the October 31st-November 1st case from the "Lille 88" field experiment [13]. This case was chosen since surface temperature falls very rapidly as night falls and stays below the freezing point during most of the night, as can be seen in Figure 3.

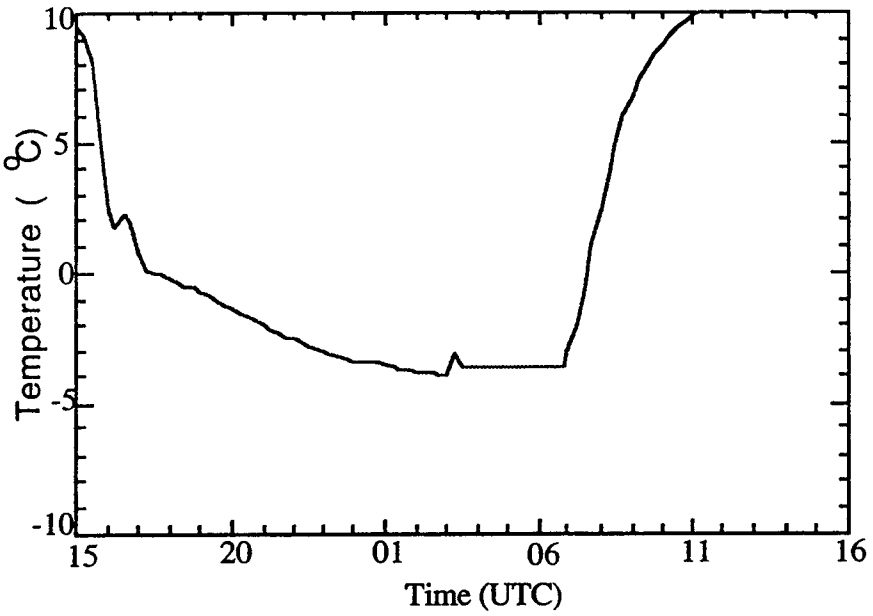

Figure 3. Simulated surface temperature for the October 31st-November 1st "Lille 88" case, from 1500 UTC October 31st to 1500 UTC November 1st.

Furthermore, Bergot [8] describes this case as a "near fog" event, meaning that a dense fog layer did not materialize even though early evening atmospheric conditions at the experimental Carnin site (Nord-Pas de Calais region, northern France) suggested a very strong probability that a dense fog layer would form during the night.

In his study, Bergot [8] showed the importance of parametrizing, in a realistic fashion, the *dewfall* process (and thus the *frost deposition* process, also) for a successful simulation of this particular "near fog" event. It should be pointed out that Bergot defines a dense fog event as a night during which the observed horizontal visibility is reduced below 200 m during a period of more than 1 1/2 hours. If these conditions are not met, the case is then considered as a "no fog" event.

To illustrate the impact of the frost deposition parameterization scheme, twenty-four-hour simulations were performed with and without the corrections presented in Section 2.1. Thus, comparisons will show the differences between one simulation where the dew deposition parameterization is used even though the surface temperature falls below the freezing point and the other simulation where the frost deposition is taken into account. Since surface observations did not show any significant advection over the site, these parameters were set to zero for the present simulations. Geostrophic winds (pressure forces) are taken from forecasts provided by the then operational French PERIDOT model [14]. Horizontal visibility is computed as a function of liquid water content [15]. Simulations are initialized at 1500 UTC October 31st and end at 1500 UTC November 1st. Figure 4 presents the results concerning the simulated horizontal visibility near the surface. It is observed that when the dew deposition parameterization is used instead of the frost deposition parameterization, the model simulates the formation of a dense fog layer (visibility below 200m) in the latter hours of the night (from 0300 UTC to 0715 UTC November 1st) (Figure 4 (a)). When the frost deposition process is taken into account, instead of dew deposition, the simulated horizontal visibility stays just above 200 m during the entire night (Figure 4 (b)). Consequently, it is concluded that the model successfully simulates the non-formation of a *dense* fog layer. This result obtained with the frost deposition parameterization is closer to the observed reality, as quoted from Bergot when describing observations at the experimental Carnin site: "relative humidity stays close (or equal) to 100 percent near the ground but a dense fog layer did not develop" [8].

Figure 5 shows the modeled relative humidity at the lowest model level for the same two simulations. During the first hours of the night (period highlighted in both figures), it can be observed that the relative humidity obtained with the frost deposition deposition parameterization (Figure 5 (b)) is a few percent lower than the one obtained with the dewfall parameterization (Figure 5 (a)). This results from a more important downward water vapor flux when the frost deposition parameterization is used. In fact, for the period highlighted in Figure 5, an increase of about 30 percent in the intensity of the surface latent heat flux has been diagnosed when the frost deposition parameterization is used as compared to the simulation where dew deposition is considered. Also, it should be mentioned that similar tests were performed without considering the e_{is}/e_{ws} correction *in the linearization procedure* of the surface water vapor flux (eqs. (2), (3) and (4)). This results in using $(\partial q_{sat}/\partial T)$ instead of $(\partial q_{satfrost}/\partial T)$ in eq. (3). Results obtained with and without the correction to the linearization procedure showed no significant differences. Consequently, this suggests that this correction, in other words the use of eq. (4), could be omitted when computing the surface frost deposition.

It can then be concluded that an increased downward water vapor flux (frost deposition) leads to an increased depletion of the atmospheric water vapor content near the surface, thus lowering the total amount of condensable water vapor that can possibly be transformed into liquid water under the influence of continuous cooling. Finally, tests performed showed that the version of the model incorporating the previously described frost deposition parameterization is able to simulate the process thought to be responsible for the occurrence of an observed near-fog event.

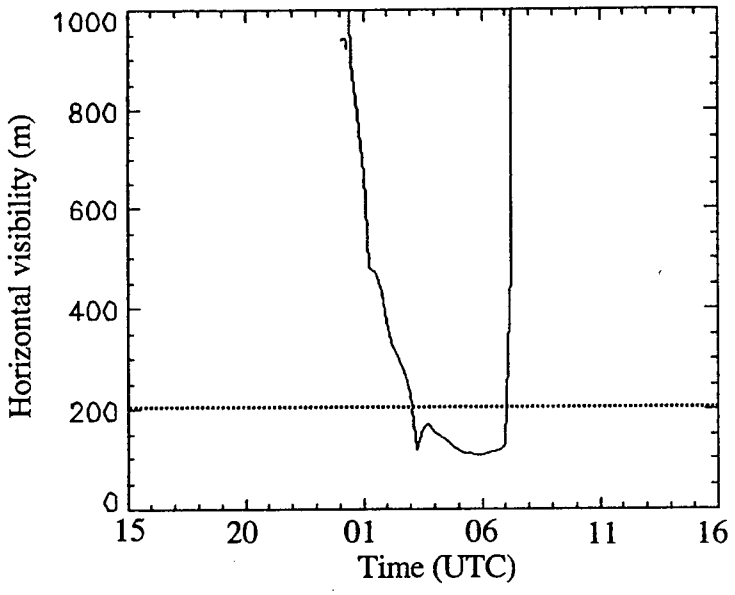

(a)

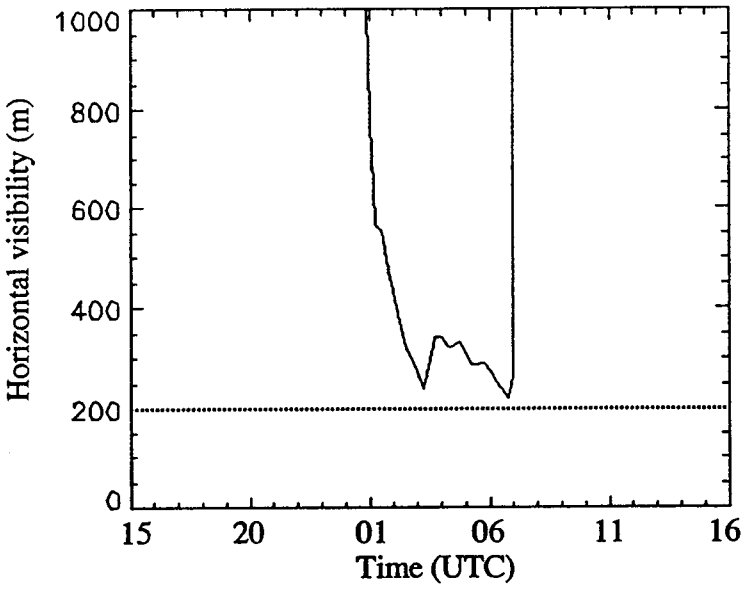

(b)

Figure 4. Simulated horizontal visibility at the lowest model level (0.5 m) for the October 31st-November 1st "Lille 88" case, from 1500 UTC October 31st to 1500 UTC November 1st, (a) without and (b) with the frost deposition parameterization.

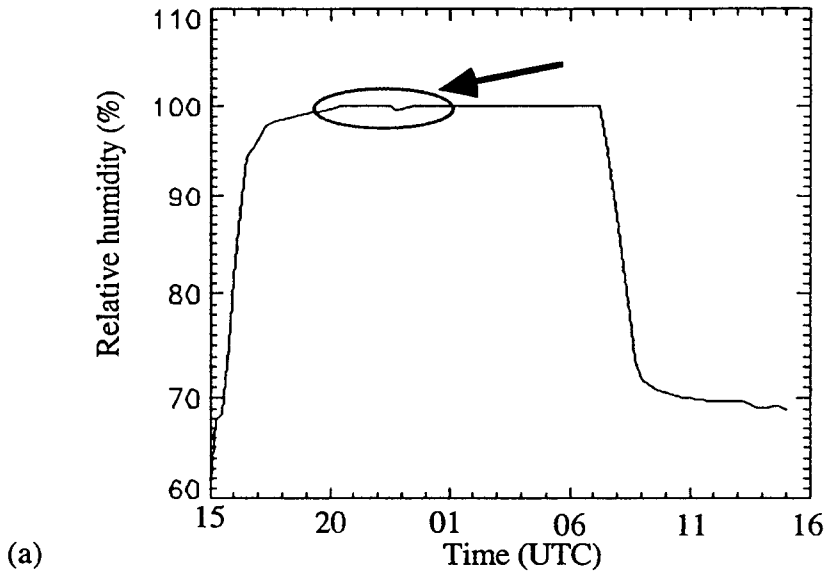

(a)

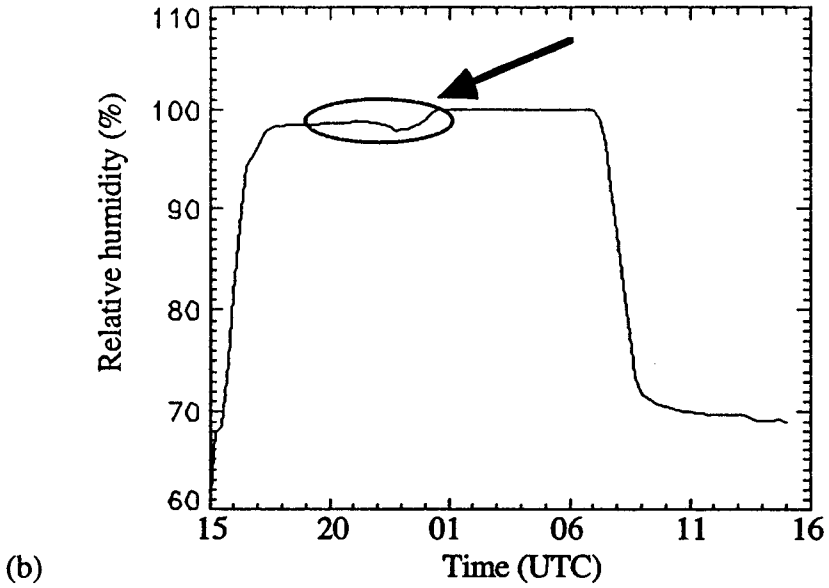

(b)

Figure 5. Simulated relative humidity at the lowest model level (0.5 m) for the October 31st-November 1st "Lille 88" case, from 1500 UTC October 31st to 1500 UTC November 1st, (a) without and (b) with the frost deposition parameterization.

3.2 Other Modifications

To study the impact of modifications, described in Sections 2.2 and 2.3, to the COBEL code used at UQAM and to make sure that previously drawn conclusions (see [8] and [4]) can still be verified, a simulation performed with the version of the model incorporating all modifications described above was compared with previous results. Here, the November 15th-16th "Lille 88" case was selected since it is characterized by a dense fog layer [8], which became fairly deep toward the end of the night. The overall synoptic situation can be described as follows. A large anti-cyclone centered over the Nord-Pas de Calais region in France, with a central surface pressure of 1030 hPa, was slowly moving toward the east. Light easterly winds and a cirrus cloud cover can further describe the meteorological conditions over the region of interest. An important cooling rate at the surface after sunset led to the lowering of the horizontal visibility below 1000 m starting around 2230 UTC November 15th and ultimately to the formation of a dense fog at about 0100 UTC on November 16th. Regional surface observations suggested very weak advections of temperature and humidity. For this reason, these external forcings were set to zero in the following integrations. Geostrophic winds are again provided by the PERIDOT model. Here, two twenty-four-hour simulations were performed, with and without the previously described modifications, so that comparisons could be made. Both simulations were initialized at 1500 UTC November 15th.

Figure 6 shows the results of these simulations by presenting modeled time evolution of the vertical profile of liquid water mixing ratios. By looking at these results, virtually no differences can be observed, thus suggesting that implemented modifications have no major impact on the simulated fog layer. But when actually computing the differences between results of both simulations, differences become more clearly observable as shown in Figure 7. When looking at contours (every 1x10^{-4} Kg m^{-3}) representing differences ("with" modifications minus "without") in the time evolution of the vertical profile of liquid water mixing ratio (Figure 7 (a)), we see that very little differences are observed during the first few hours of the simulation (from 1500 UTC November 15th to 0600 UTC November 16th). In fact, differences stay below 1x10^{-4} Kg m^{-3} . This period corresponds to the formation and mature phases of the fog layer, which has been studied by [8], *thus suggesting that conclusions drawn by him can still be considered valid.*

But later in the simulation, profiles of differences in the liquid water content are weakly negative in the lower part of the fog layer and positive in the upper part as shown in Figure 7 (b). This phenomenon becomes more apparent with time, thus suggesting that liquid water is transported upward at a faster rate in the simulation performed with the modified version. This seems to be related to a more important turbulence mixing within the fog layer for the simulation performed with the modified version of the COBEL code. Figure 8 shows the *difference* between the turbulent fluxes of liquid water, as diagnosed in the simulations with and without the modifications (difference-> "with" minus "without"), for the period where most important differences in liquid water contents are observed (0200 to 1200 UTC November 16th). Since a positive (upward) flux is expected at the top of the fog layer, positive values near cloud top indicate that the upward flux of liquid water is larger when the modified version is used. Negative values in the lower part of the layer indicate that the downward flux is also larger (more negative) with the newest version, since a negative (downward) flux is occurring in that part of the layer.

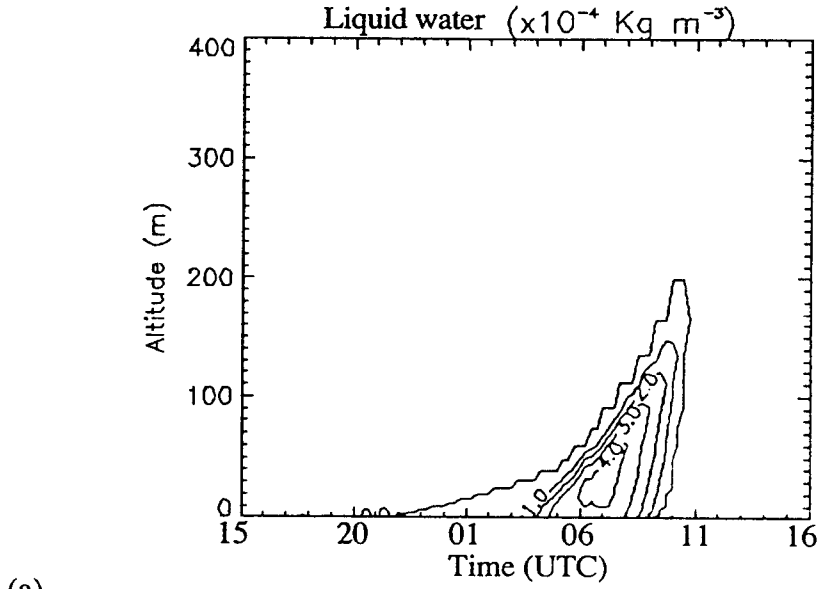

(a)

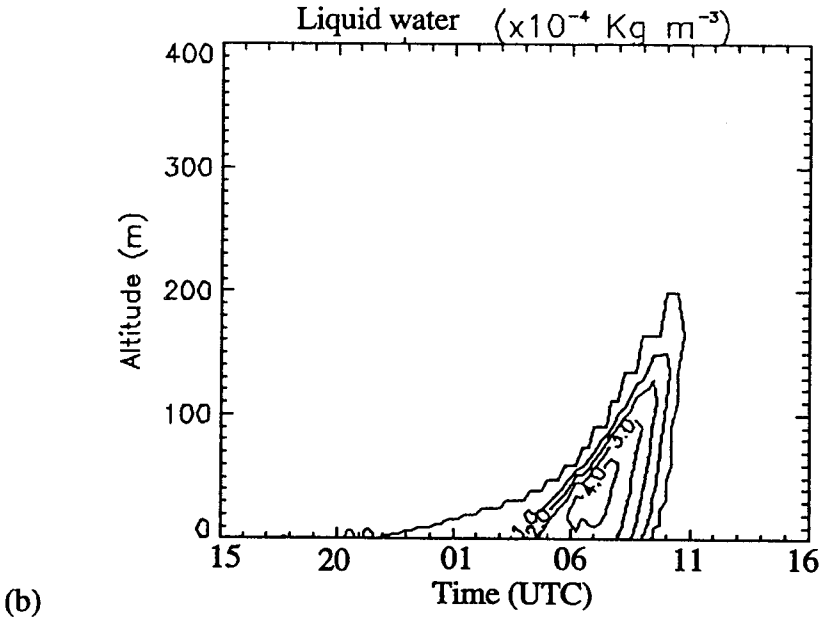

(b)

Figure 6. Simulated time and space variation of the liquid water mixing ratio for the November 15th-16th "Lille 88" case, from 1500 UTC November 15th to 1500 UTC November 16th, (a) without and (b) with the modifications described in Sections 2.2 and 2.3.

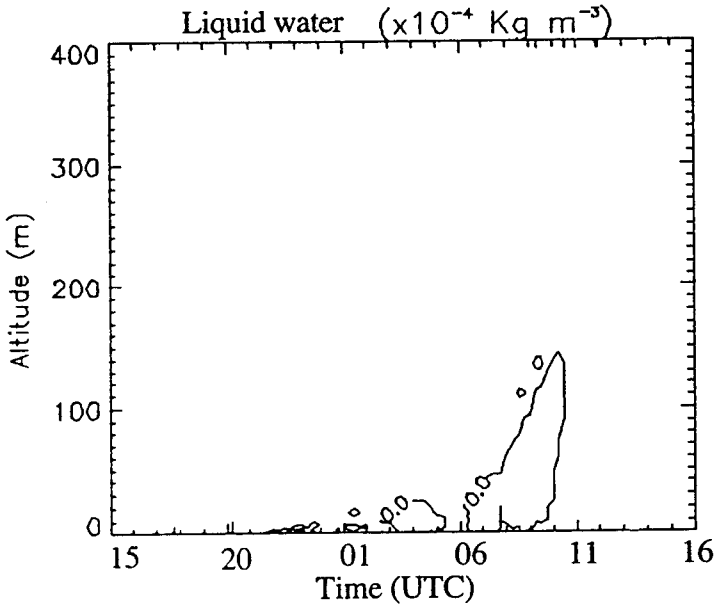

(a)

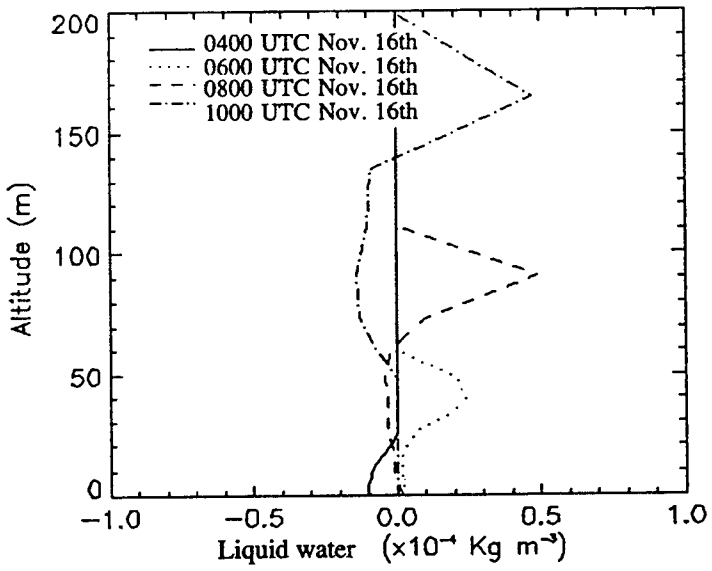

(b)

Figure 7. Time and space variation (a) and vertical profiles at different times (b) of differences in liquid water mixing ratio for simulations with and without the modifications described in Section 2 (latest minus previous model versions), for the November 15th-16th "Lille 88" case.

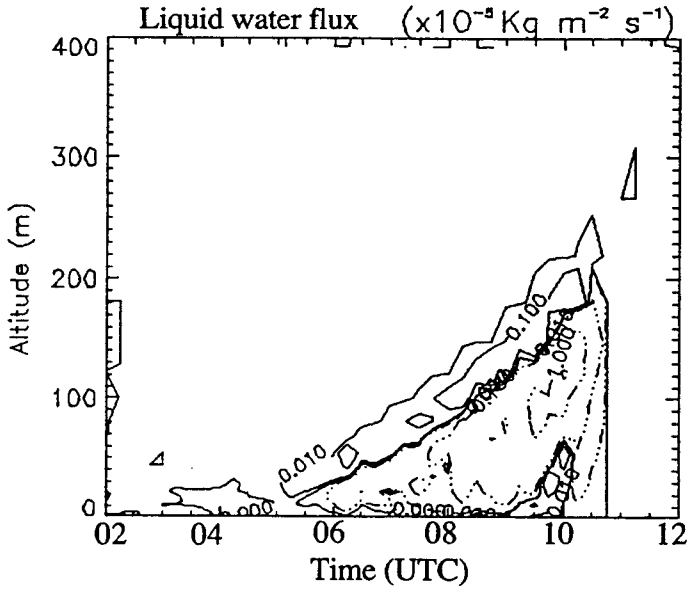

Figure 8. Time and space variation of differences in liquid water flux for simulations with and without the modifications described in Section 2 (latest minus previous model versions), from 0200 UTC to 1200 UTC November 16th. Simulations were initialized at 1500 UTC November 15th. Solid lines indicate positive values, while dotted lines indicate negative values. Drawn contours are (-1, -0.1, -0.01, 0, +0.01, +0.1, +1) 10^{-5} Kg m^{-2} s^{-1}.

This increase in the turbulent mixing is due to differences in the diagnosed stability within the fog layer. Corrections to the computation of stability apparently lead to a diagnosis of less stable or more unstable layers near fog top, leading to more turbulent diffusion of liquid water in that region. To illustrate this fact, Figure 9 shows, as an example, the diagnosed profile of stability within the fog layer at 0600 UTC November 16th for simulations performed before (old) and after (new) the corrections were implemented. This time was chosen since it is the time just before noticeable differences appear in modeled liquid water mixing ratios (see Figure 7 (a)). It should be noted that negative values denote unstable layers, and inversely positive values indicate the presence of stable layers. We see that the most apparent differences are located near fog top, where less stable layers are diagnosed with the corrected formulation of stability in a saturated atmosphere. The same characteristics are found later in the simulations (at 0830 UTC November 16th; Figure 10) when less unstable layers are diagnosed near the surface and, again, less stable ones appear near fog top, thus leading to continuously more important upward diffusion of liquid water at fog top in the simulation performed with the described modifications to the COBEL code.

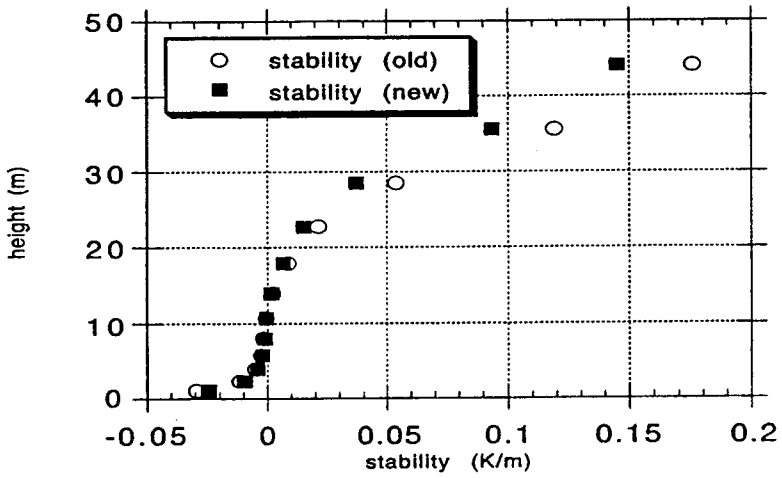

Figure 9. Vertical profile of stability within the fog layer at 0600 UTC November 16th for simulations with (new) and without (old) the modifications described in Section 2.

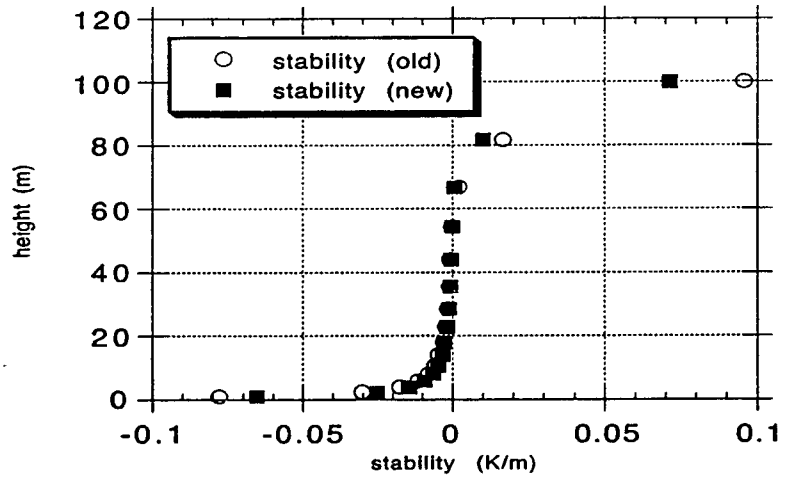

Figure 10. Vertical profile of stability within the fog layer at 0830 UTC November 16th for simulations with (new) and without (old) the modifications described in Section 2.

Now, to clearly show that implemented modifications do not affect the capability of the model to forecast a fog layer's onset and early evolution with the accuracy shown in Bergot's study [8], Figure 11 shows a comparison of the simulated evolution of horizontal visibility at 1.6 m with the observed one at 1.4 m at the Carnin site on the evening of November 15th and night of the 16th, 1988. We see that the observed evolution of visibility is quite well reproduced. The predicted fog onset time is approximately the same as the observed one, but the sudden drop in visibility observed around midnight (hour 24) happens a little earlier in the simulation. Nevertheless, low visibilities observed from 0130 to 0300 UTC November 16th are remarkably

well reproduced. This suggests that, again, Bergot's results are still verified with our slightly modified version of the COBEL model.

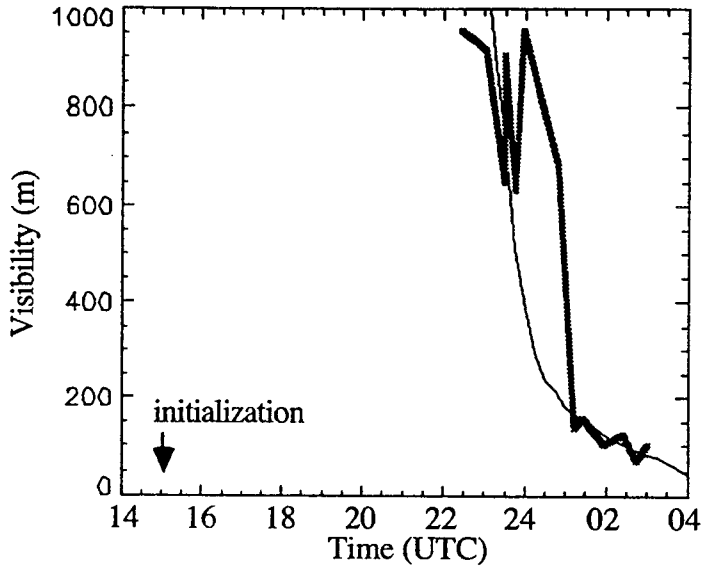

Figure 11. Time evolution of modeled (thin line) horizontal visibility at 1.6 m and observed visibility (thick grey line) at 1.4 m (adapted from fig. V.27 (d) of Bergot, 1993), for the 15th-16th November "Lille 88" case (Model initialization: hour 15 = 1500 UTC November 15th).

4. ADDITIONAL MESOSCALE EXTERNAL FORCINGS

The initial formulation of the COBEL model included horizontal advections of temperature and humidity as external forcings [1]. To improve COBEL's coupling with the mesoscale environment, the effects of pressure tendencies and vertical motion (w=dz/dt) have been introduced in COBEL's 1D simulations. These effects are thought to be of utmost importance in the representation of the low cloud field and thus to the very short-term prediction of C&V events. For instance, local pressure tendencies modify the saturation state of an air parcel by changing its temperature (adiabatic compression or expansion). Thus, motionless humid air parcels can theoretically be brought to saturation only under the influence of local pressure falls, thus resulting in the formation of fog or stratus. Also, advection by the vertical wind component (w) plays an important role in determining the structure of the BL by, for example, maintaining or strengthening the capping inversion at the top of the BL in the case of subsidence. This inversion, by its strength and vertical location (i.e., height relative to the Lifting Condensation Level), plays an important role in the maintenance or dissipation of a stratocumulus cloud deck [16]. Consequently, both forcings can act on a column of air and help determine the cloud amount in that column. For this reason, pressure tendencies and vertical motion have been added as complements to the set of external forcings "driving" the COBEL column model. Horizontal advections of horizontal winds (u and v) and of pressure were also implemented in the model but have not yet been tested. For this reason, these topics will not be extensively discussed here.

For very short-term forecasting, all external forcings can be obtained from detailed mesoscale analyses of mesoscale numerical weather prediction models such as the Canadian Regional Finite Element (RFE) or Mesoscale Compressible Community (MC2) models, the National Meteorological Center's Rapid Update Cycle (RUC) or ETA models, the National Center for Atmospheric Research/Pennsylvania State University MM5 model or the Colorado State University RAMS model.

4.1 Local Pressure Tendency

4.1.1 Implementation

The introduction of pressure tendencies in the model implies that the pressure profile used during a COBEL simulation can be variable. In the initial formulation of the model, the surface pressure was set constant to a value of 1000 hPa and the vertical pressure profile was obtained by solving the hydrostatic equation using the initial temperature profile. This pressure profile was kept constant throughout an integration. Since COBEL is formulated using the potential temperature θ, it should be pointed out that the use of a surface pressure of 1000 hPa implied that the potential temperature θ at the surface is equal to the surface sensible temperature T since the definition of θ is :

$$\theta = T\left(\frac{1000\,\text{hPa}}{p}\right)^{R/c_p} \qquad (10)$$

Consequently, θ or T could be used in an interchangeable manner in the surface energy budget equation without any further consideration. This simplified quite a bit the coupling, within COBEL, of the atmosphere with the ground.

But considering that a variable pressure profile should be a part of the COBEL model, the surface pressure will most probably be different than the previously standard 1000 hPa value. Therefore, some additional modifications needed to be implemented in the model code to preserve the consistency of the model's soil-atmosphere coupling. To summarize, the energy budget equation was reformulated in terms of the potential temperature θ instead of the temperature T. The soil heat diffusion equation was rewritten in a "pseudo soil potential temperature" θ_s. This "pseudo potential temperature" is defined as:

$$\theta_s(z_s)=T_s(z_s)\left(\frac{1000\,\text{hPa}}{p_{sfc}}\right)^{R/c_p} \tag{11}$$

where z_s is the depth within the ground. θ_s is initialized using equation (11) for every model level defined by the grid within the ground. It should be mentioned that this change of variable has no physical significance. It is solely an artificial mathematical trick to eliminate the use of fictitious gradients between the atmospheric potential temperature θ and the soil sensible temperature T, which appear when the surface pressure is different than 1000 hPa, in the computation of surface heat fluxes. Using the above definition, the soil heat diffusion equation becomes:

$$\frac{\partial\theta_s}{\partial t}=\frac{\partial}{\partial z}\left(\frac{k_s}{\rho c_p}\frac{\partial\theta_s}{\partial z}\right)-\frac{\theta_s R}{p_{sfc}c_p}\frac{\partial p_{sfc}}{\partial t} \tag{12}$$

It can be observed that equation (12) is quite similar to the usual form of the diffusion equation [17], apart from an additional "correction" term. This correction term arises from the change of variable and is a function of the surface pressure (p_{sfc}) tendency (second term on the right of (12)).

With these modifications, all heat fluxes are computed in terms of a potential temperature and are thus "transparent" to the value of surface pressure, meaning that a surface pressure value different than 1000 hPa can now be used, provided that potential temperatures are computed and used properly.

Now from the atmospheric point of view, COBEL computes the evolution of the potential temperature, *a conserved quantity in an adiabatic atmosphere*. Thus pressure changes in the column of air act mainly to modify the saturation state of a layer by modifying its temperature (T), and thus its associated saturation water vapor mixing ratio $q_{sat}(p,T)$. Within COBEL's algorithm, for a given time step, the potential temperature equation is solved first to obtain θ at time $t+\Delta t$, then the water vapor mixing ratio equation (q at $t+\Delta t$), then both equations for the wind components are solved. Only then, the "new" (at $t+\Delta t$) sensible temperature is computed from the "new" potential temperature, using the following relation,

$$T(z)=\theta(z)\left(\frac{p(z)}{1000\ \text{hPa}}\right)^{R/c_p} \tag{13}$$

to compute the "new" saturation mixing ratio $q_{sat}(p,T)$ using equation (9). A check is then made to see if supersaturation (or sub-saturation in the case where liquid water is already present) is attained. If a phase change is required (liquid to vapor or vapor to liquid), the "all or nothing" condensation scheme is then applied to determine the new equilibrium state defined as T* and q* (see [6]). θ* is then computed from T* and we are ready to go on to the next time step.

With this algorithm in mind, it was decided that the pressure tendencies should intervene to modify the pressure profile just before the computation of the new temperature T and of $q_{sat}(p,T)$. The following equation is thus added at this point:

$$p^{t+\Delta t} = p^t + \left(\frac{\partial p}{\partial t}\right)^t \Delta t \tag{14}$$

where the pressure tendency can be obtained from analyses or the output of a mesoscale model. Equation (14) is applied to all model levels, including the surface. This way, for a given time step, changes of the saturation state of air parcels related to pressure changes in the column are taken into account when computing the condensation/evaporation term in the liquid water budget equation. Thus mesoscale pressure changes now contribute to the representation of BL clouds within COBEL.

4.1.2 Validation

The validation of the above described modifications is again based on the simulation of the November 15th - 16th "Lille 88" fog case. First, an integration was performed with the modified version using an identical set-up as was used with the initial version of the model (i.e., surface pressure of 1000 hPa and no pressure tendency). A comparison could then be made with previous results in order to acquire the confidence that implemented modifications did not introduce artificial effects that would degrade the quality of simulations. Results were identical to those obtained with the initial version (results not shown).

The next step toward the validation of the new capabilities of the model is to compare Bergot's simulation of this case [8] with results obtained with our modified version, using the true value of 1030 hPa for the surface pressure (instead of Bergot's 1000 hPa). To simplify the validation process, *no pressure tendencies are applied* for this integration (pressure profile constant during the whole simulation). Here, twelve-hour simulations are used since the focus is on the formation stage of the fog layer. Figure 12 presents the results of near surface horizontal visibility obtained with pressure profiles computed from surface pressure values of 1000 hPa and 1030 hPa, respectively. It is observed that the lowering of the visibility below 1000 m occurs about one hour earlier for the integration performed with p_{sfc}=1030 hPa, compared to the one where p_{sfc}=1000 hPa. Also, the poorest visibility value attained after twelve hours of integration is about 50 m lower when a 1030 hPa value is used instead of 1000 hPa. This can be explained by the fact that the use of a higher surface pressure will lead to higher pressure values throughout the column and thus, with the same initial temperature values, leads to a lower value of the overall saturation mixing ratio (eq. 9).

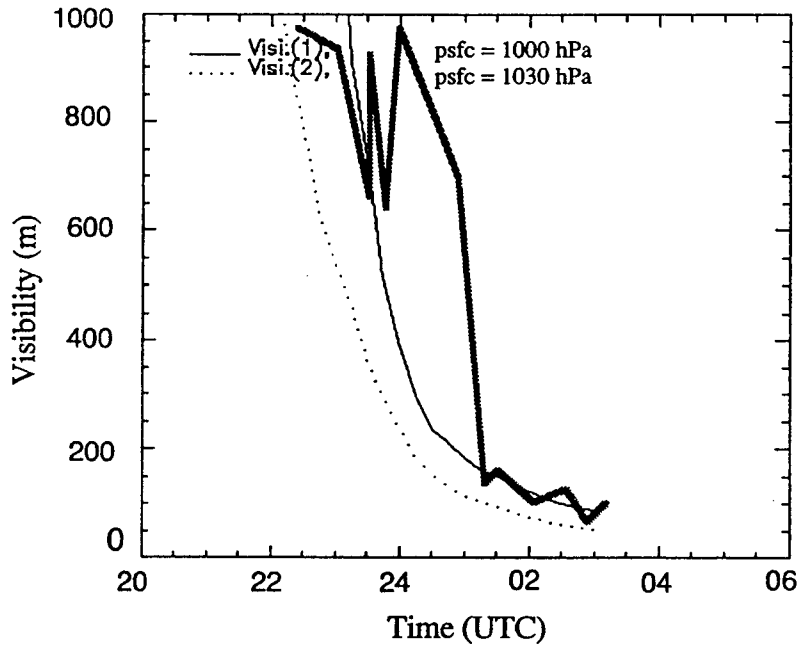

Figure 12. Time evolution of modeled horizontal visibility at 1.6 m using 1000 hPa as surface pressure (thin solid line), 1030 hPa (dotted line) and observed visibility (thick grey line) at 1.4 m (adapted from fig. V.27 (d) of Bergot, 1993), for the 15th-16th November "Lille 88" case. Model initialization performed at 1500 UTC November 15th.

Consequently, the initial state of the present integration is characterized by a higher relative humidity and hence saturation is attained sooner when the cooling rate is the same, as is the case here. It can also be observed that with the real surface pressure measured at the experimental site, the simulated fog layer appears earlier and is somewhat denser at the end of the integration when compared to observations. Nevertheless, these discrepancies are relatively small in the present context and results can be considered reasonably accurate.

After validating the modifications related to the possible use of various surface pressure values, the modifications related to the implementation of *temporal* variations of the pressure profile, a simulation was performed while applying a very small pressure tendency throughout the column and throughout the integration. This way, significant differences with the reference simulation (no pressure tendency) are not to be expected. A value of -0.01 hPa/3h has been chosen for the experiment. A surface pressure of 1030 hPa was used for the reference simulation and the test simulation as well. No significant differences were observed between results (not shown) when carefully studying the model output. So, it can be concluded with fairly good confidence that the chosen approach for the implementation of pressure tendencies in the COBEL model is working according to expectations. This will be further verified through sensitivity experiments.

4.1.3 Sensitivity Experiments

In this section, results of experiments concerning the sensitivity of the model to pressure tendencies are presented. Simulations were performed with various values of pressure tendencies and results are compared to the reference simulation characterized by no pressure tendency. Firstly, the November 15th - 16th "Lille 88" fog case is used, with an initial surface pressure value of 1030 hPa. Secondly, using the same data from the November 15th - 16th "Lille 88" fog case as a framework, a hypothetical stratus case was constructed by artificially "injecting" some additional humidity in the upper portion of COBEL's grid. The initial specific humidity profile was modified so as to obtain a relative humidity oscillating around 95 percent between 200 m and 950 m. Experiments conducted with these conditions will be presented and discussed later in this section.

First, concentrating on the fog case, pressure tendencies of -3 hPa/3h, -1 hPa/3h, +1 hPa/3h and +3 hPa/3h were applied during COBEL integrations. This range of values is considered reasonable and not entirely uncommon in a number of meteorological conditions. For every experiment, each pressure tendency value was applied throughout the column and throughout the twelve-hour integrations.

Figure 13 shows comparisons of horizontal visibility, at 1.6 m, between the reference simulation and simulations performed with -1 hPa/3h and -3 hPa/3h pressure tendencies. As expected, the fog layer appears earlier when pressure is falling. For a tendency of -1 hPa/3h (Figure 13 (a)), significant condensation occurs about 1/2 hour earlier than in the reference case. In fact, the significant visibility reduction starts at 2145 UTC when the tendency is applied compared to 2215 UTC in the reference simulation. The rate at which visibility reduction occurs is about the same at first but becomes less important as the visibility approaches its minimum. This is mainly due to the fact that as the fog layer becomes thick enough; IR radiation emitted within the fog produces some heating that counteracts the surface cooling. At the end of the integration, horizontal visibilities are close to each other in both simulations. When a -3 hPa/3h tendency is applied (Figure 13 (b)), the same characteristics are observed as in the previous experiment (-1 hPa/3h) but with more pronounced differences with the reference case. The horizontal visibility first reaches the 1000 m threshold about 1 hr 15 min earlier than in the reference case. A much more important visibility reduction is observed between 2100 UTC November 15th and 0130 UTC November 16th. At the end of the twelve-hour integration, the visibility is about 40 m lower when pressure falls were applied.

When positive pressure tendencies are applied, the fog layer appears some time later than in the reference case (Figure 14). In fact, the significant visibility reduction (visibility below 1000 m) occurs 3/4h and 1 3/4h later when +1 hPa/3h and +3 hPa/3h pressure tendencies are applied, respectively (Figure 14 (a) and 14 (b), respectively). At the end of the integration, the visibility is only about 50 m higher when the +1 hPa/3h tendency was applied compared to the reference case, but is about 150 to 200 m higher when a +3 hPa/3h was applied. In fact, in this latter case a dense fog layer (visibility below 200 m) never appeared after twelve hours of integration.

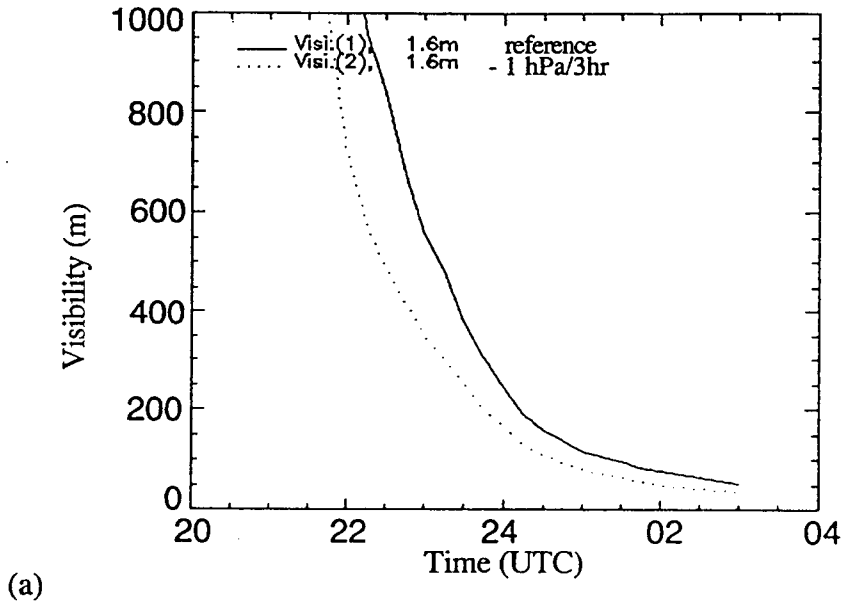

(a)

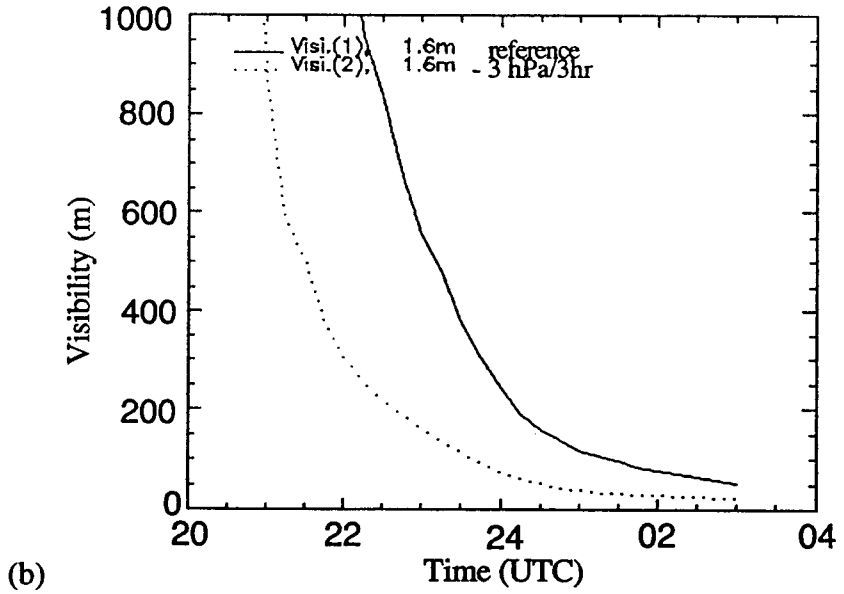

(b)

Figure 13. Time evolution of modeled horizontal visibility at 1.6 m with (a) -1 hPa/3h and (b) -3 hPa/3h. The reference case is shown with a thin solid line and test cases are shown with a dotted line. Model initialization performed at 1500 UTC November 15th.

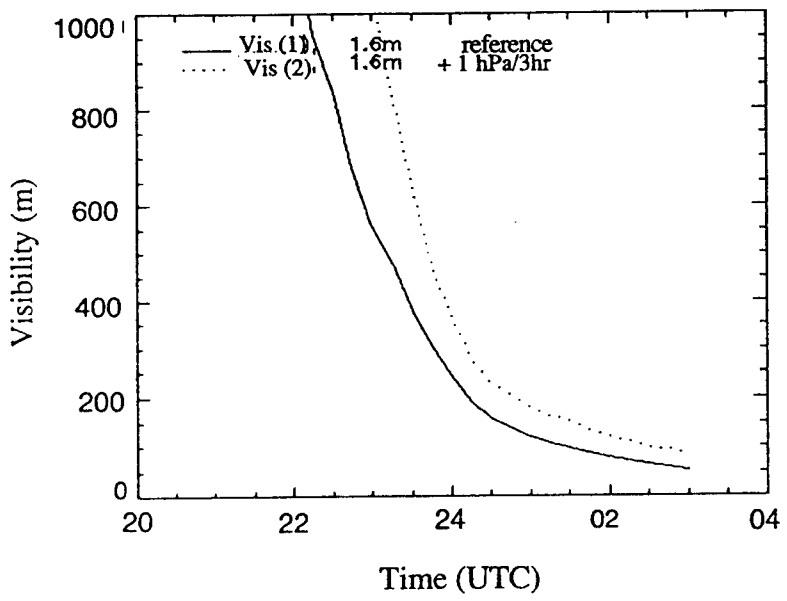

(a)

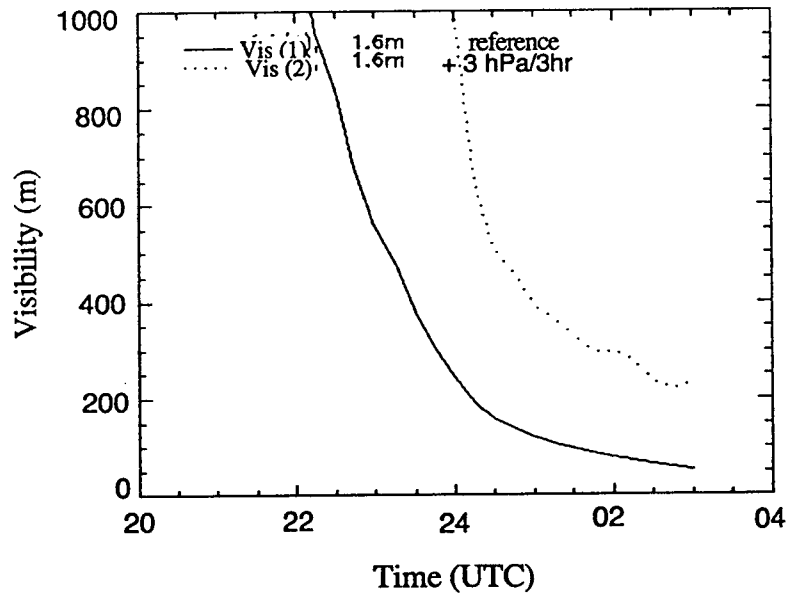

(b)

Figure 14. Time evolution of modeled horizontal visibility at 1.6 m with (a) +1 hPa/3h and (b) +3 hPa/3h. The reference case is shown with a thin solid line and test cases are shown with a dotted line. Model initialization performed at 1500 UTC November 15th.

Now studying the impact of pressure tendencies on the *vertical extent* of a fog layer, Figure 15 shows the resulting temporal evolution of the liquid water content profile with +3 hPa/3h, 0 hPa/3h (reference case) and -3 hPa/3h pressure tendencies. It is shown that the evolution of the

fog layer is quite sensitive when different pressure tendencies are applied. For the reference case (Figure 15 (b)), the maximum height reached by the saturated layer after twelve hours of integration is 40 m, compared to 20 m and 60 m when +3 hPa/3h (Figure 15 (a)) and -3 hPa/3h (Figure 15 (c)) pressure tendencies are applied, respectively.

These simple experiments have shown that the appearance and evolution of a fog layer is quite sensitive to the adiabatic cooling/warming induced by local pressure tendencies. Fog onset shows a variability of the order of about one hour for pressure tendency values that are commonly observed in the real atmosphere. Also, it has been shown that the height of a fog layer can be doubled when a relatively moderate negative pressure tendency (falling pressure) is present.

Now, in order to study the impact of pressure tendencies on BL cloud layers, the initial specific humidity profile of the November 15th -16th "Lille 88" case was modified by adding some humidity in the 200 m - 950 m layer so that the relative humidity became close to 95 percent in that domain. Then, simulations were made with 0 hPa/3h, -1 hPa/3h and -3 hPa/3h pressure tendencies. Here, only results from the -3 hPa/3h experiment are shown since in the two other experiments no cloud formed during the twelve hours of integration. Figure 16 shows the resulting temporal evolution of the liquid water content profile throughout the twelve hours of integration. It is shown that the expected fog layer forms around 2100 UTC as before (see Figure 13 (b)) and most importantly that a stratus cloud starts forming at about 2015 UTC at a height of 800 m (Figure 16 (a)). As the night progresses, this cloud thickens (increased liquid water content) and its base lowers toward the surface. Figure 16 (b) shows a "zoom" on the evolution of the fog layer. A comparison with Figure 15 (c) shows that the development of the fog layer is greatly reduced by the presence of the overlying cloud cover. The increased downward IR radiation emitted by this cloud even leads to the complete dissipation of the fog at around 2300 UTC. The present results suggest that local pressure tendencies can contribute to the formation of low level clouds and thus have a non-negligible importance in the very-short-term prediction of such clouds. Also, this experiment has permitted us to verify that the model is able to represent the interaction between a stratus/fog cloud system.

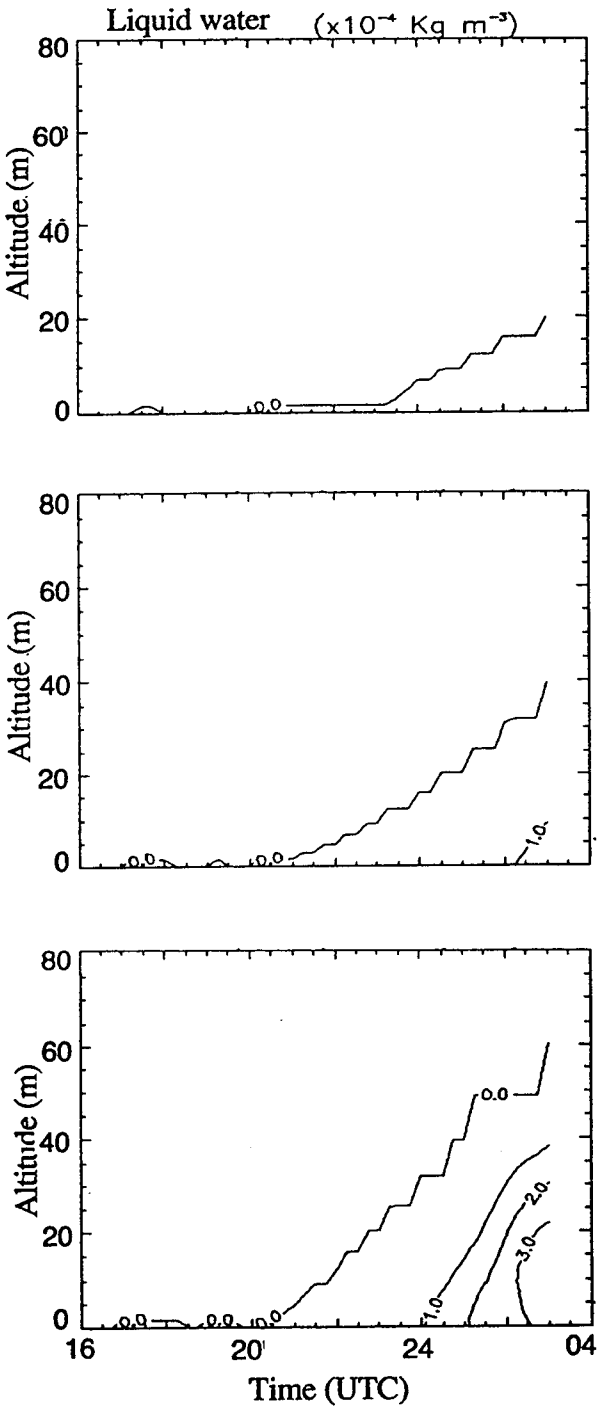

a) $\partial p / \partial t = +3\text{hPa} / 3\text{hr}$

b) $\partial p / \partial t = +0\text{hPa} / 3\text{hr}$

c) $\partial p / \partial t = -3\text{hPa} / 3\text{hr}$

Figure 15. Time evolution of modeled liquid water content profile with (a) +3 hPa/3h, (b) 0 hPa/3h and (c) -3 hPa/3h. Model initialization performed at 1500 UTC November 15th.

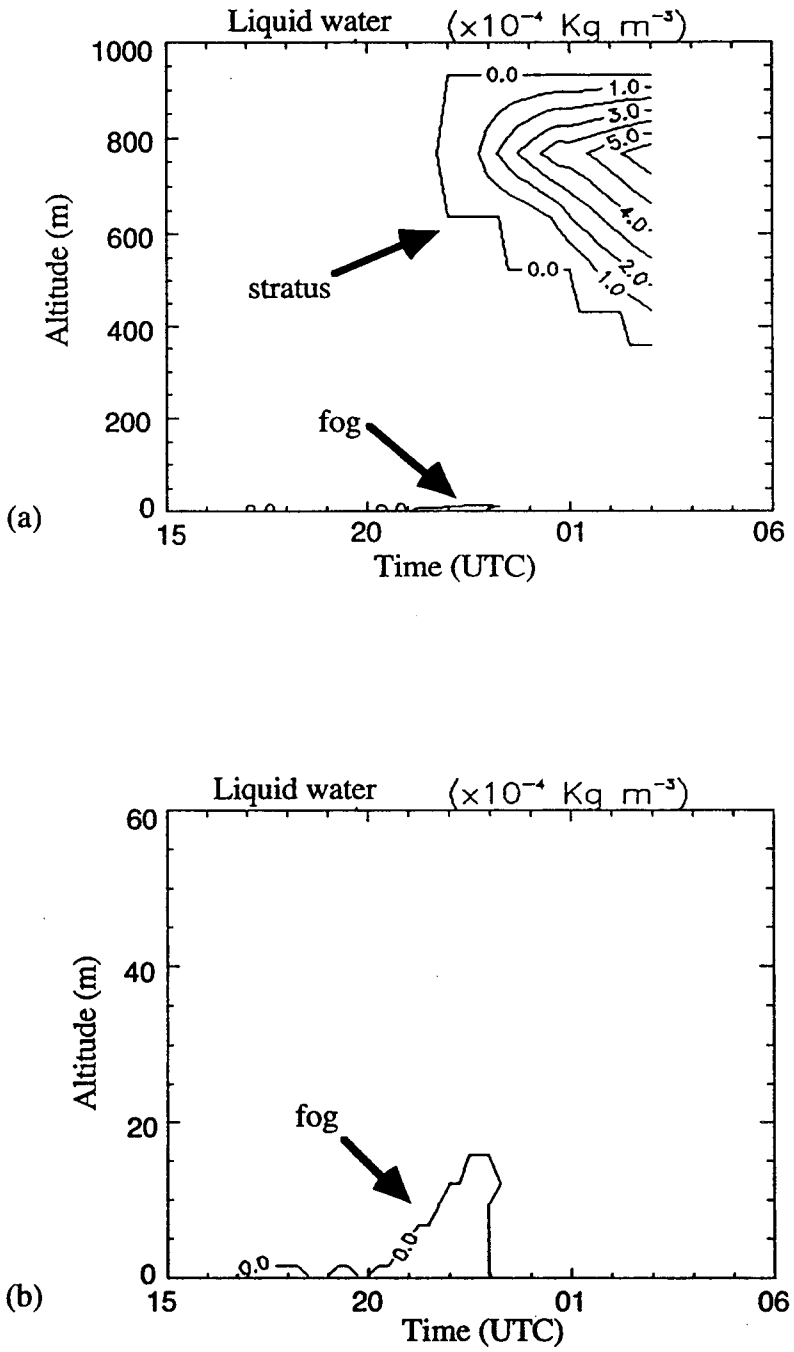

Figure 16. Time evolution of modeled liquid water content profile with -3 hPa/3h in the lowest 1 km (a) and in the lowest 60 m (b) of the atmosphere.

4.2 Vertical Motion (w=dz/dt)

Now that local pressure tendencies were implemented in the model to take into account the in-situ cooling/warming related to falling/rising pressure that may eventually lead to the formation/dissipation of clouds, advection by the vertical wind is another process to take into account to represent the cooling/warming due to the vertical displacement of an air parcel. It is recognized that synoptic scale or mesoscale vertical velocities are often at least an order of magnitude lower than convective vertical velocities generally found within the convective boundary layer and thus can be considered negligible. But this is not the case in the stable nocturnal boundary layer. Also, subsidence plays an important role in maintaining the inversion capping the boundary layer. The "strength" and height of this inversion is regulated by this mesoscale subsidence and has a direct influence on the boundary layer cloud cover. Thus, vertical advection needs to be implemented within the model to hope for a realistic representation of the cloud-topped boundary layer.

4.2.1 Implementation

The three-dimensional advection of a variable α can be written as:

$$\vec{V} \cdot \vec{\nabla} \alpha = \vec{V}_h \cdot \vec{\nabla}_h \alpha + w \frac{\partial \alpha}{\partial z} \qquad (15)$$

where the first term on the right is the horizontal component while the second term is the vertical component of the overall advection. The horizontal advection of potential temperature and water vapor mixing ratio was already included in the COBEL model, as discussed in [6]. The vertical component can be calculated by using the vertical motion "w" taken from a mesoscale model or computed from analyses, and is thus an external parameter, and by computing the vertical derivative of α within the 1D model (internal parameter). This method has been chosen, instead of computing the entire term externally, to be consistent with the objective of taking advantage of COBEL's high vertical resolution.

For now, vertical advection terms have been added to equations governing the evolution of both horizontal velocity components (u and v), potential temperature, water vapor mixing ratio and liquid water mixing ratio. Vertical advection of turbulent kinetic energy has been omitted for now.

A suitable numerical method has to be identified in order to represent vertical advection as accurately as possible. This topic alone has been extensively discussed in the literature over the past several years. Several schemes with various degrees of complexity exist but all have undesirable characteristics such as false dispersion or dissipation [18]. But here, simplicity is an important quality to consider. Due to the uncertain nature of possible impacts related to these characteristics in our context, two simple schemes have been chosen and implemented in the model to verify if solutions obtained with both schemes do not diverge significantly. The goals of this exercise are to, first, help in the selection of one of the two schemes and, second, to assess the sensitivity of the model to the choice of the advection scheme.

The first considered scheme is the "forward-in-time, upstream-in-space" scheme [19], while the other is the "forward-in-time, centered finite difference" or Euler scheme [20]. The first

scheme is dissipative and thus its use may result in some degradation in the representation of fine-scale features. The second scheme is dispersive. The main undesirable effect related to the use of this latter scheme in the COBEL model is the possible appearance of unphysical negative water vapor and liquid water content. These unphysical "holes" can be eliminated with the use of simple "hole filling" algorithms. But the use of these algorithms can result in some artificial transport of liquid water or water vapor.

4.2.2 Validation

Various twenty-four-hour simulations were carried out to compare results obtained with both schemes. The November 15th-16th "Lille 88" fog case, as well as the "stratus" case obtained by modifying the initial humidity profile of the former case, have been used. In all simulations, a 1030 hPa surface pressure has been used, with no pressure tendencies. Figure 17 shows the used vertical motion profile. This profile is characterized by a relatively small constant value of +0.2 cm/s in the major part of the domain, diminishing to 0 cm/s at the ground. All simulations have been initialized at 1500 UTC November 15th (day 1) and stopped at 1500 UTC November 16th (day 2).

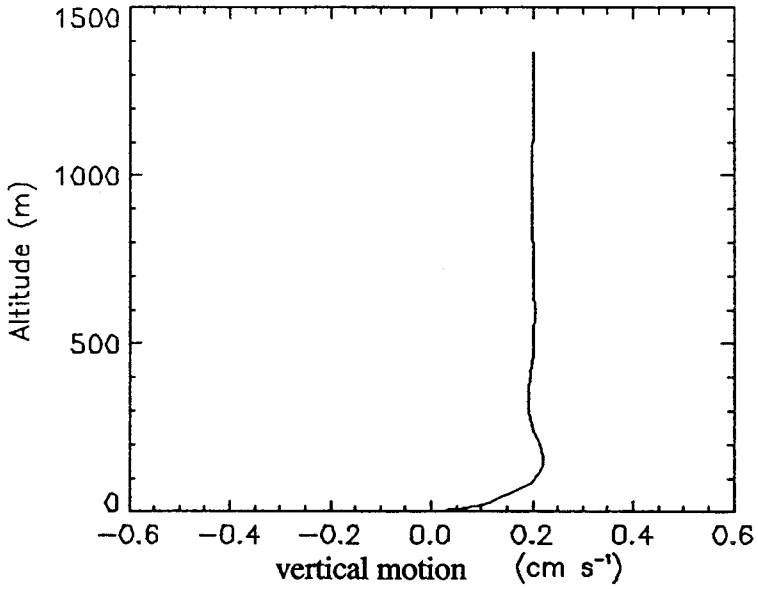

Figure 17. Vertical profile of vertical motion used in COBEL simulations.

First, two *temporal* differencing methods have been tested for both schemes. Explicit and implicit versions have been coded and tested. Here, explicit and implicit means that the vertical derivative in the second term of equation (15) is considered at time "t" or "t+Δt", respectively. Results (not shown) indicate that simulated liquid water contents obtained when using the two advection schemes are almost identical, thus suggesting that with our short time step (60 sec. and 30 sec. when liquid water has appeared), the temporal differencing is not an important factor when considering vertical advection algorithms. The implicit formulation was then chosen to be

consistent with the already coded implicit formulation of the sedimentation flux divergence term in the liquid water budget equation. When using a constant sedimentation velocity, as is the case here (see [6]), this term becomes an "advective" term (velocity times the gradient of the field) :

$$\frac{\partial G}{\partial z}=\frac{\partial v_i q_l}{\partial z}=v_i\frac{\partial q_l}{\partial z}\left(\text{if } v_i=\text{cte}\right) \qquad \textbf{(16)}$$

where $G = v_i q_l$ is the sedimentation flux of cloud droplets. Since this term contributes to the vertical advection of liquid water, it is believed that a uniform or consistent numerical differencing between this term and the implemented vertical advection term is preferable. Another reason for choosing the implicit formulation is the unconditionally stable nature of the scheme. With an explicit formulation, great care must be taken to ensure that the Courant-Friedrichs-Levy criterion [20] is met to eliminate the possible appearance of spurious unstable numerical modes.

Now concentrating on the *spatial* differencing of the two tested schemes, again several simulations have been carried out. Implicit versions of the "upstream" and "centered finite difference" schemes were used in separate simulations and resulting liquid water contents were compared. Possible negative liquid water contents are eliminated by simply setting values back to zero whenever negative values appear. For the fog case, differences between results are minimal due to the fact that the fog layer is located below 100 m and that the magnitude of the vertical motion in that layer is very small (results not shown). For the hypothetical "stratus" case, significant differences are observed. It can be seen in Figure 18 that the adiabatic cooling due to the upward motion leads to the formation of a cloud deck initially at a height of about 900 m. Overnight, cloud base lowers probably due to the sedimentation of cloud droplets. What is remarkable here is the difference in the time of formation of the cloud layer when different vertical advection schemes are used. When the "centered finite difference" advection scheme is used, the cloud layer appears roughly three hours earlier than when the "upstream" scheme is employed.

The following question is then raised: Which scheme is more accurate? Since the "centered finite difference" scheme is of the second order and the "upstream" is a first order scheme, the former should be more accurate. To verify this, the resolution in the upper part of COBEL's grid was improved. The original grid was distributed according to a log-linear relationship which resulted in a considerable decrease in resolution toward the top of the model domain [6]. A constant grid spacing of 60 m was implemented by adding 10 levels above 300 m, while preserving the original high resolution of the grid below that level. This resulted in a minimal increase in the computer cost. Figure 19 shows results obtained with this new configuration of the grid. Apart from the fact that more details can be observed in the evolution of the cloud layer, it can be seen that results obtained with both vertical advection schemes tend to converge toward the same solution. The time of formation of the cloud layer obtained with the "centered finite difference" scheme is again between 1800 and 1900 UTC, while the one with the "upstream" scheme has changed from 2200 UTC to 2000 UTC. The fact that the solution toward which the results seem to converge closely resembles the one obtained with the "centered finite difference" advection scheme in the previous experiment (original grid, Figure 18) suggests that this scheme is the most accurate of the two, as suspected. Consequently, this scheme is retained for the experiments to follow, as well as the new grid configuration.

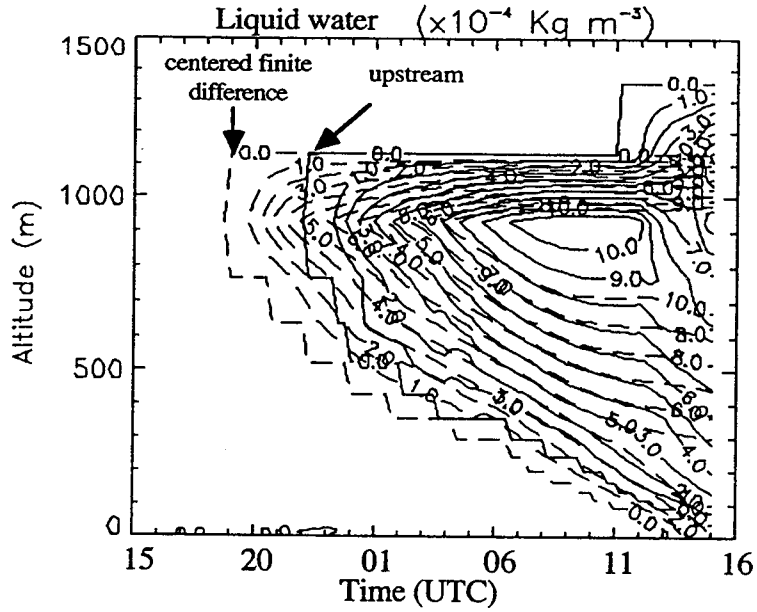

Figure 18. Time evolution of the liquid water content profile for the hypothetical stratus case, from 1500 UTC on day 1 to 1500 UTC on day 2. Results obtained with the "centered finite difference" scheme are shown with a dashed line, and those obtained with the "upstream" scheme with a solid line.

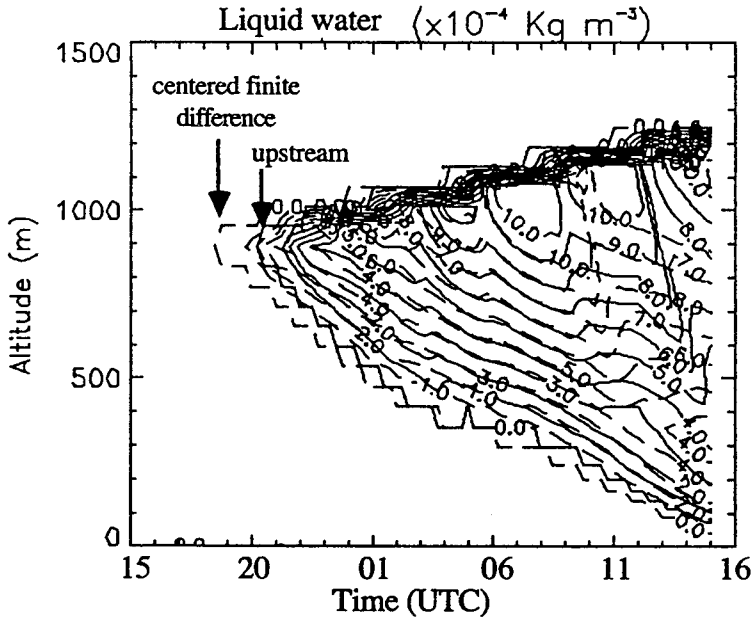

Figure 19. Time evolution of the liquid water content profile for the hypothetical stratus case, with the new grid configuration, from 1500 UTC on day 1 to 1500 UTC on day 2. Results obtained with the "centered finite difference" scheme are shown with a dashed line, and those obtained with the "upstream" scheme with a solid line.

4.2.3 Sensitivity Experiments

Now that an advection scheme has been chosen and that the resolution of the grid has been improved, a set of experiments were undertaken to assess the sensitivity of COBEL simulations to vertical motion. Again, simple experiments were performed on the November 15th-16th "Lille 88" fog case described previously and the hypothetical stratus case used in the validation process of the implementation of vertical advection terms. Various twenty-four-hour simulations were performed by imposing no vertical motion, upward vertical motion, and downward vertical motion. Simulations have been initialized at 1500 UTC November 15th (day 1) and stopped at 1500 UTC November 16th (day 2). The profile shown in Figure 17 is used for the simulation when ascending motion is imposed while its mirror image is used when imposing downward motion, meaning that a -0.2 cm/s vertical motion is present over most of the domain. For each experiment, the vertical motion profile is set constant throughout the simulation.

Figure 20 shows results of the experiment performed on the fog case. Note that the vertical domain of each graph is different. What is most apparent in this figure is that the time of fog onset is independent of the vertical motion. But the vertical extent of the simulated fog layer is very sensitive. With fairly weak vertical velocities, the evolution of the fog layer is quite different. For instance, the maximum height of the fog layer reached during the twenty-four-hour simulations is 26 m, 250 m and 475 m when downward motion, no motion and upward motion have been imposed, respectively. When subsidence was imposed, the fog layer even dissipated completely in the morning at about 0800 UTC (Figure 20 (a)) while a fog-to-stratus transition occurred in the morning when no vertical motions were applied, with complete stratus burn-off around 1130 UTC (Figure 20 (b)). It should be noted that for the date considered (November 16th), sunrise takes place at about 0715 UTC in northern France. When upward motion is applied, no fog/stratus complete burn-off occurs in the morning (Figure 20 (c)). Only a decrease in the liquid water content is observed in the lowest 200 m starting at sunrise. Unfortunately, no solid conclusions can be drawn at this point concerning comparisons with *reality* for the burn-off time as mesoscale forcings (geostrophic winds, advections, high-cloud cover etc.) were not available beyond a twelve-hour forecast (beyond 0300 UTC November 16th). For our experiments, these missing forcings for the last twelve hours of our simulations were simply set constant to their last available values.

For the hypothetical "stratus" case, results of significance have already been shown. When no vertical motion is applied, essentially no stratus cloud layer appears during the simulation, thus permitting the fog layer to grow as shown in Figure 20 (b). When subsidence is imposed, again no stratus cloud appears due to the adiabatic warming related to the downward motion. A limited growth of the fog layer then takes place near the surface as shown in Figure 20 (a). In the case where weak upward motion was imposed, the resulting liquid water field evolution is shown in Figure 19. Again, slight variations in the vertical motion forcing imposed within a COBEL simulation produces quite different results.

Even though the hypothetical context employed here prevents any serious comparisons with reality, these results suggest that the presence of even small vertical motions, advecting basic meteorological quantities, have a non-negligible effect on the outcome of low cloud events, which is of great importance to aviation traffic management.

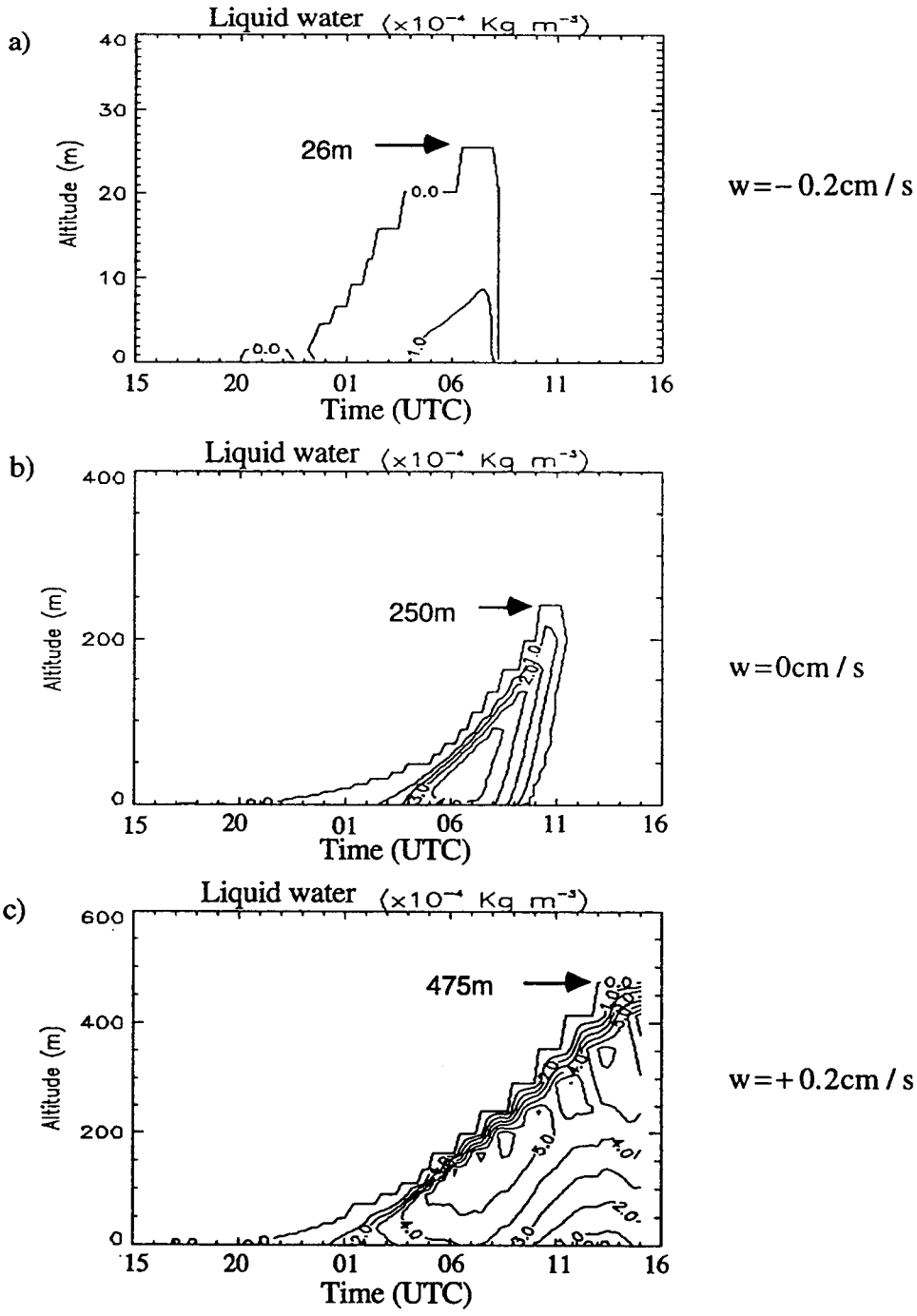

Figure 20. Time evolution of the liquid water content profile for the fog case, from 1500 UTC on day 1 to 1500 UTC on day 2, with (a): -0.2 cm/s, (b): 0 cm/s and (c): +0.2 cm/s.

4.3 Other Implementations

4.3.1 Horizontal Advection of Horizontal Winds

Since vertical motion is associated with the divergence of horizontal winds, through the continuity equation [17] and thus to horizontal gradients of horizontal winds, it may be preferable to implement the terms representing horizontal advection of horizontal momentum in the 1D simulation to better keep track of the three-dimensional distribution of momentum. No significant tests have been undertaken to verify this statement, but nevertheless these terms have been added as possible external forcings used to drive the COBEL model. These forcings have been implemented following the guidelines of Bergot [8] (see also [6]) for the computation of horizontal advection terms.

4.3.2 Horizontal Advection of Pressure

To complement the introduction of effects related to the variability of the pressure field, the contribution of the horizontal advection of pressure term has also been implemented. Near the surface, an air parcel being horizontally advected in a region characterized by an important horizontal pressure gradient might experience significant cooling/warming due to the imposed adiabatic expansion/compression. As suggested by results obtained within the "eulerian" point of view of in situ pressure tendencies, this "lagrangian" change of pressure may play an important role in the formation/dissipation of fog or stratus. Since COBEL uses potential temperature as a prognostic variable, this effect can be introduced in our 1D simulations by modifying the computation of the horizontal advection of potential temperature. Using the standard definition of potential temperature θ, the horizontal advection of θ can be written:

$$\vec{V}_h \cdot \vec{\nabla}_h \theta = \frac{\theta}{T}\left[\vec{V}_h \cdot \vec{\nabla}_h T\right] - \frac{R}{c_p}\frac{\theta}{p}\left[\vec{V}_h \cdot \vec{\nabla}_h p\right] \qquad (17)$$

already in the model — newly implemented

The initial formulation of the model incorporated only the first term on the right of (17). Since COBEL uses potential temperature as one of its prognostic variables, the advection of sensible temperature was computed from mesoscale analyses or from a mesoscale model and incorporated within the 1D simulation using this truncated version of equation (17). Now, the possibility of using the complete form of (17) has been coded in the model. Thus, the horizontal advection of pressure computed from analyses of a model can be incorporated in a COBEL simulation, but no significant tests have been performed. Consequently, no further discussion concerning this topic will be presented here.

5. APPLICATION OF COBEL TO AVOSS SUPPORT

In the U.S., the most immediate operational application in which COBEL could be of potential value would be in support of a wake vortex hazard system, such as the Advanced VOrtex Spacing System (AVOSS). Wake vortices generated by leading aircraft represent a hazard for other aircraft which may encounter these trailing vortices while taking off or landing. Thus, wake vortex behavior represents an important safety concern for ATC personnel. Evidence suggests that current wake-vortex-imposed aircraft spacing restrictions may be unduly conservative during most situations that compel IFR operations. Since spacing between aircraft directly affects airport capacity, improved wake vortex advisories could yield significant cost savings [21].

It is only when wake vortices are relatively long lived that they represent a potential threat. The atmospheric environment, especially in the lower boundary layer, is an important factor in determining whether wake vortices are likely to be an operational concern. An AVOSS could benefit significantly from accurate predictions of the transition between stable and mixed boundary layer regimes. These transitions, usually occurring during the morning and evening hours, can dramatically alter the vertical structure of the horizontal wind. Such information would provide useful support to detailed, timely gridded winds analyses in the terminal area that would reveal whether wake vortices will linger in the approach path or be blown away. For example, when the boundary layer stabilizes late in the day, the atmosphere near the surface may become "decoupled" from that above, resulting in a calming of the wind that can occur rather abruptly. The opposite sequence of events, with a sudden increase in the wind, is often observed during the morning transition. These times often correspond to peak periods in airport demand.

While the COBEL technology would contribute significantly to a wake vortex advisory system such as the AVOSS if only it could predict the stabilizing and destabilizing of the boundary layer, COBEL would also provide other potentially useful information. For example, COBEL produces predictions of both turbulent kinetic energy, a parameter depicting the mean strength of turbulent motions, and boundary layer thermal stratification. Theoretical studies have determined that atmospheric turbulence leads to rapid dissipation of wake vortices and that they are also affected by the vertical stratification of the atmosphere [22].

6. SUMMARY

Experiments conducted in France showed that the use of the coupled COBEL-mesoscale model forecasting system results in an important improvement in the quality and accuracy of radiation fog forecasts [3]. This initial work, performed by Paul Sabatier University in Toulouse, France under funding from Météo-France, is an especially good example of leveraging in technology transfer.

Building on the capabilities demonstrated by COBEL in France, UQAM has enhanced the model so that a wider range of meteorological phenomena can now be represented. These improvements are relevant to the ITWS goal of developing products to support automated short-term predictions (nowcasts) of operationally significant C&V events. The most significant improvements included incorporating:

- A parameterization for surface frost formation;
- The effect of saturated air on atmospheric stability (fog);
- Additional non-local large-scale forcing components;
- The local pressure tendency; and
- Advection by the vertical wind component.

These factors influence the overall boundary layer environment, especially the onset, evolution and dissipation of fog and stratus. Experiments showed that when these influences were omitted there was more of a problem on somewhat longer time scales (12 to 24 hours) and suggest that some error would likely be seen in the finer details on shorter time scales (0 to 6 hours).

Column models have been used successfully to represent the current state and the very-short-term evolution of the lower atmospheric in the terminal area [23]. This development has lead to a prototype operational Oregon State University (OSU) column model, forced by measured surface fluxes, that is currently implemented in support of MIT Lincoln Laboratory's San Francisco International Airport Stratus Project. COBEL has shown encouraging results in representing the evolution of the fine-scale vertical structure of the lower boundary layer in general and that of the stable nocturnal boundary layer in particular. COBEL's ability to model the evening transition from the neutral to the stable regime with light winds is the main feature behind its success in predicting radiation fog in northern France [8]. Preliminary studies have shown that COBEL is also able to realistically represent the stable to neutral transition occurring in the morning [4]. Furthermore, [24] has studied the processes linked to the evolution of the wind maximum at the top of the stably stratified boundary layer (low level jet). Her work suggests that COBEL incorporates the physics necessary to realistically simulate the onset and subsequent evolution of the low level jet. Nocturnal low level jets have been frequently observed at Dallas/Ft. Worth, a principal candidate for an AVOSS demonstration.

Future development efforts will concentrate on the operational implementation of COBEL. UQAM is already completing the development of a graphical user interface to support COBEL's

display requirements within an operational environment. In France, initial data sets will be provided by the operational mesoscale model run by Météo-France and additional sensors that will supplement an automated surface observation system similar to the ASOS in the U.S. For ITWS applications, the initial vertical structure and surface forcing can be provided by the flux-forced OSU column model supplemented by ITWS sensor data. The Swedish weather service is working on an automated terminal aviation forecast system based on a column model that appears to provide additional techniques for specifying initial conditions [25]. Finally, there is the option of developing a flux-forced version of COBEL. Since it would be less straightforward to implement this capability for COBEL than it was for the OSU column model, this effort should await evaluation of its performance with its current design.

GLOSSARY

$\vec{\nabla}$	gradient vector operator
$\vec{\nabla}_h$	horizontal gradient vector operator
$\vec{V}_h$	horizontal wind vector
$\vec{V}$	wind vector
1D	one-dimensional
3D	three-dimensional
AVOSS	Advanced VOrtex Spacing System
BL	boundary layer
C&V	ceiling and visibility
C_h	exchange coefficient
cm	centimeters
COBEL	COde Brouillard Eau Liquide
C_{pa}	specific heat at constant pressure of dry air
C_{pv}	specific heat at constant pressure of water vapor
c_p	specific heat at constant pressure
d/dt	total derivative operator (with respect to time)
DFW	Dallas/Ft. Worth International Airport
E	surface water vapor flux
ECMWF	European Centre for Medium-range Weather Forecast
e_{is}	saturation vapor pressure over ice
ETA	NMC's model in ETA coordinates
e_{ws}	saturation vapor pressure over liquid water
FAA	Federal Aviation Administration
F_c	ratio of latent heat of sublimation and latent heat of evaporation
G	sedimention flux of cloud droplets
GCSS	GEWEX Cloud System Study
Γ_d	dry adiabatic lapse rate
Γ_m	pseudo-adiabatic lapse rate
g	grams
g	gravitational acceleration
h, hr	hour
hPa	hectopascals
Hu	surface relative humidity parameter
$Hu_{depo.}$	surface relative humidity parameter (for dew deposition)
$Hu_{evap.}$	surface relative humidity parameter (for evaporation)
IFR	instrument flight rules
ITWS	Integrated Terminal Weather System
kg	kilograms
km	kilometers
k_s	soil thermal conductivity
L, L_v	latent heat of evaporation
LES	Large Eddy Simulation

L_s	latent heat of sublimation
MC2	Mesoscale Compressible Community model
MIT/LL	Massachusetts Institute of Technology Lincoln Laboratory
MM5	Mesoscale Model version 5
m	meters
min	minutes
NMC	National Meteorological Center
OSU1DPBL	Oregon State University column model
^oC	degrees Celcius
PÉRIDOT	Prévisions à Échéances Rapprochées Intégrant des Données Observées et Télédétectées
p	atmospheric pressure
p_{sfc}	atmospheric pressure at the surface
θ	potential temperature
q	water vapor mixing ratio
q^*	equilibrium water vapor mixing ratio
q_l	liquid water mixing ratio
θ_s	soil "potential" temperature
q_{sat}	saturation mixing ratio (with respect to liquid water)
$q_{satfrost}$	saturation mixing ratio (with respect to ice)
q_w	total water mixing ratio
q_{z1}	water vapor mixing ratio at lowest model level
R, R_d	gas constant of dry air
RAMS	Regional Atmospheric Modeling System
RFE	Regional Finite Element model
RUC	Rapid Update Cycle model
R_v	gas constant of water vapor
ρ	air density
ρ_s	soil density
SFO	San Francisco International Airport
s	seconds
T	atmospheric temperature
T^*	equilibrium temperature
TKE	Turbulent Kinetic Energy
T_s	soil temperature
T_{so}	soil surface temperature
t	time
UQAM	Université du Québec à Montréal
UTC	Universal Time (Greenwich mean time)
u	zonal wind component
v	meridional wind component
v_i	sedimentation velocity
w	vertical motion in height coordinates
z	hight above ground
z_s	depth within the soil
$\partial/\partial t$	partial derivative operator (with respect to time)
Δ	finite difference operator

REFERENCES

[1] Bergot, T. and D. Guédalia, 1994: "Numerical forecasting of radiation fog. Part I: Numerical model and sensitivity tests," *Mon. Wea. Rev.*, **122**, pp.1218-1230.

[2] Guédalia, D. and T. Bergot, 1994: "Numerical forecasting of radiation fog. Part II: A comparison of model simulations with several observed fog events," *Mon. Wea. Rev.*, **122**, pp.1231-1246.

[3] Bergot, T. and D. Guédalia, 1995: "Évaluation de la qualité de la prévision du brouillard par un modèle numérique," Submitted to *La Météorologie*.

[4] Tardif, R. and P. Zwack, 1994 : *Toward a General Boundary Layer Model for Aviation Weather Forecasting Applications: A Report on COBEL Improvements*, Internal report, Département de Physique, Université du Québec à Montréal, presented to Massachusetts Institute of Technology Lincoln Laboratory.

[5] ECMWF, 1993: *ECMWF/GCSS Workshop on the Parameterization of the Cloud Topped Boundary Layer*, European Centre for Medium-Range Weather Forecasts, 8-11 June 1993, Shinfield Park, Reading, U.K.. Available from ECMWF.

[6] Tardif, R., T. Bergot, D. Guédalia and P. Zwack, 1994: *COBEL: Description of a One-Dimensional Boundary Layer Model for Radiation Fog Forecasting*, Internal report, Département de Physique, Université du Québec à Montréal, presented to Massachusetts Institute of Technology Lincoln Laboratory.

[7] Fouquart, Y. and B. Bonnel, 1980: "Computations of solar heating of the Earth's atmosphere: a new parameterization," *Beitrage zur Physik der Atmosphare*, **53**, pp.35-62.

[8] Bergot, T., 1993: *Modélisation du Brouillard à l'Aide d'un Modèle 1D Forçé par des Champs Mésoéchelle: Application à la Prévision.* Thèse de Doctorat, Université Paul Sabatier, Toulouse, France, N° d'ordre 1546, 191 pp.

[9] Rapport de D.E.A. Astrophysique, Géophysique et Techniques spatiales, Université Paul Sabatier, Toulouse, France, 51 pp.

[10] Rogers, R. R. and M. K. Yau, 1989: *A Short Course in Cloud Physics*, Pergamon Press, Toronto, 293 pp.

[11] Durran, D., and J. B. Klemp, 1982: "On the effects of moisture on the Brünt-Väisälä frequency," *J. Atmos. Sci.*, **39**, pp.2152-2158.

[12] Triplet, J.P. and G. Roche, 1977: *Météorologie Générale*, 2nd edition, Ecole Nationale de la Météorologie, Paris, 317 pp.

[13] Guédalia, D. and T. Bergot, 1992: "Premiers résultats de la campagne Lille88 d'étude du brouillard," *La Météorologie*, 7e série, **42**, pp.11-20.

[14] Imbard, M., A. Joly and R. Juvanon du Vachat, 1986: "Le modèle de prévision PERIDOT. Formulation dynamique et modes de fonctionnement," *Note de travail de l'E.E.R.M.* no **161**, Météo-France, Toulouse, France.

[15] Kunkel, B., 1984: "Parameterization of droplet terminal velocity and extinction coefficient in fog model." *J. Appl. Meteor.*, **23**, pp.34-41.

[16] Kloesel, K. A., 1992: "Marine stratocumulus cloud clearing episodes observed during FIRE," *Mon. Wea. Rev.*, **120**, pp.565-578.

[17] Pielke, R. A., 1984: *Mesoscale Meteorological Modeling*, Academic Press, Boston, 612 pp.

[18] Ostiguy, L. and J. P. R. Laprise, 1990: "On the positivity of mass in commonly used numerical transport schemes," *Atmos-Ocean*, **28**, pp.147-161.

[19] Lee, T. Y., 1984: *A Numerical Study of Coastal Stratus Cloud in a Two-Dimensional Meso-Scale Model*, Ph.D. Thesis, Oregon State University, Corvallis, OR, USA, 139 pp.

[20] Haltiner G. J. and R. T. Williams, 1980: *Numerical Prediction and Dynamic Meteorology*, Second edition, John Wiley & Sons, New York, 477 pp.

[21] Evans, J. E. and J. D. Welch, 1991: "Role of FAA/NWS Terminal Weather Sensors and Terminal Air Traffic Automation in Providing a Vortex Advisory Service," FAA International Wake Vortex Symposium, October 29-31, 1991.

[22] Green, G. C., 1986: "An approximate model of vortex decay in the atmosphere," *J. Aircraft*, 23, 1986.

[23] Keller, J. L., C. Smith and F. W. Wilson, 1995: "Applications of column models for terminal weather forecasts," *Sixth Conference on Aviation Weather Systems*, American Meteorological Society, Dallas, TX, pp.66-71.

[24] Estournel C., 1988: *Etude de la Phase Nocturne de la Couche Limite Atmospherique*, Thèse de Doctorat, Université Paul Sabatier, Toulouse, France, 176 pp.

[25] Gollvik, S. and E. Olsson, 1995: A one-dimensional interpretation model for detailed short range forecasting. Meteor. Appl., 2, 209-216.